UNIVERSITY OF CALIFORNIA,
IRVINE

Exploring Aspects of Q-balls

DISSERTATION

submitted in partial satisfaction of the requirements
for the degree of

DOCTOR OF PHILOSOPHY

in Physics

by

Yahya Almumin

Dissertation Committee:
Professor Arvind Rajaraman, Co-Chair
Professor Michael Ratz, Co-Chair
Professor Mu-Chun Chen

2024

DEDICATION

To Hawraa, Mama, Baba, Mama Hajiya, Baba Haji and Waleed

Contents

List of Figures

List of Tables

ACKNOWLEDGMENTS

"You Will Never Walk Alone" is Liverpool Football Club's slogan, my favorite football club. As cliche as it sounds, it is the perfect embodiment of my journey. I am extremely privileged through out my life and career for being surrounded by people who stood by my side in my journey, and for that I will always be grateful.

Firstly, I would like to express my gratitude to my co-advisors Professor Arvind Rajaraman and Professor Michael Ratz for all their guidance, patience and support. Professor Arvind Rajaraman concentration on academic productivity, pragmatism, and honesty accelerated my academic and personal development in ways I could not have imagined. My transition from a student to a researcher was only possible because of the way he pushed me from day one. My single-author paper, the biggest milestone I achieved during my time at UCI, is a result of Professor Rajaraman's instance that I achieve academic independence during my time as PhD student. Being co-advised by Professor Michael Ratz also facilitated my academic and personal growth in a unique way as well. His firm belief that academic advancement is only possible by continues collaboration and communication between researchers has influenced me and my colleagues greatly. Professor Ratz translated his belief by connecting to us, his younger students, on a personal level. He tried to understand our exact goals, and aspirations and advised us accordingly. Professor Ratz always insisted that my colleagues and I attend seminars, summer schools, and conferences to connect with scientists all around the world to explore new topics and make more connections. This created an environment where, us, the younger scientists were able to thrive and contribute meaningfully to research in the presence of senior scientists. This can be seen in the work we were able to produce together. On a personal level, Professor Ratz company during lunch time in the Bander Room, and coffee hours was a joyful highlight of my time at UCI.

I am very thankful for all my senior collaborators whom I had the privileged to work with on various topics as well. Working on Modular Symmetries with Professor Mu-Chun Chen and Professor Saul Ramos-Sanchez was a very pleasant experience during the dark days of the pandemic, and for that I will always be thankful. I would also like to acknowledge the impact my collaborators Professor Julian Heeck and Professor Christopher B. Verhaaren had on me. This dissertation and my single-author paper were only possible because they allowed me to work with them on several Q-balls projects. The learning process I went through and the knowledge I accumulated through our collaboration define me as a physicist today.

I am also extremely grateful for my UCI friends, colleagues, and collaborators: Shreya Shukla, Victoria Knapp-Perez, Max Fieg, Anne-Katherine Burns, Helena Garcia, Mark Hayward, Dylan Green, Hamad Alshetaiwi, Mohammed Almajhadi, Ahmed Almuttawa, Ahmed, Muhannad Alshetaiwi for making this ride worth a while. I would also like to thank my senior colleagues Rebecca Riley and Jessica Howard for their valuable guidance through out my PhD.

Now, I get to the trickiest part of the acknowledgments section as words can not capture the immense gratitude I am feeling right now. In an absurd meaningless universe, I find myself

full of drive and my heart full of joy because of my family and best friends. This work is dedicated to you Hawraa, my wife and soulmate, for all of what you have done for me. I am forever indebted to you for leaving your family and friends, and putting your career on pause just to be with me. In the face of doubt and uncertainty, your presence filled me with confidence. Your unconditional love and unwavering support is the reason we are here today, love.

To Hanadi and Muthanna, my parents, how do I begin to describe the indescribable. But let me say this way: I owe everything I was, am, and will be to you. You instilled in me the fundamental values that define me as a person. Thus, whatever I have achieved is yours as much as it is mine. This dissertation is dedicated to you as well. And to my awesome siblings Ali, Juman, Muhannad, and Ahmad, I am so thankful for all the love and support you showed me through out my years. This would not have been possible without you.

To my best friends overseas Taha Ali, Ali Alqaffas, Ali Najem, Mohammed Jawad, and Jasem Alqaseer, thanks for staying in touch with me and putting up with my occasional rants for all these years. Despite the geographical and temporal separation, you guys always found the time for me, and for that I will forever be grateful.

I would also like to acknowledge Professor Irina Mocioiu, Professor Sarah Shandera, Professor Richard Robinett and Professor Ameenah Farhan for believing in me from the early stages in my career. Their support and guidance paved the way for me to accomplish my aspirations as a young physicist.

As you can see, I never and will never walk alone.

Thanks for Kuwait University for sponsoring my scholarship and funding my work through out grad school.

Chapter 2 is a reprint of the material as it appears in [2], used with kind permission of The European Physical Journal (EPJ). The coauthors listed in this publication are Julian Heeck, Arvind Rajaraman, and Christopher B. Verhaaren. Arvind Rajaraman directed and supervised research, which forms the basis for the dissertation.

Chapter 4 and Appendix A are a reprint of the material as it appears in [3], used with kind permission of The European Physical Journal (EPJ). The coauthors listed in this publication are Julian Heeck, Arvind Rajaraman, and Christopher B. Verhaaren. Arvind Rajaraman directed and supervised research, which forms the basis for the dissertation.

VITA

Yahya Almumin

EDUCATION

Doctor of Philosophy in Physics and Astronomy **2024**
University of California, Irvine *Irvine, CA*

Masters of Science in Quantum Fields and Fundamental Forces **2019**
Imperial College of London *South Kensington, London*

Bachelor of Science in Physics **2017**
Pennsylvania State University *State College, PA*

RESEARCH EXPERIENCE

Graduate Research Assistant **2019–2024**
University of California, Irvine *Irvine, California*

TEACHING EXPERIENCE

Graduate Teaching Assistant **2020**
University of California, Irvine *Irvine, CA*

Learning Assistant **2016**
Pennsylvania State University *State College, PA*

REFEREED JOURNAL PUBLICATIONS

On the Calculation of Invariant Tensors in Gauge Theories **2020**
Acta Physica Polonica B

Metaplectic Flavor Symmetries from Magnetized Tori **2021**
Journal of High Energy Physics

Excited Q-balls **2021**
European Physical Journal C

Neutrino Flavor Model Building and the Origins of Flavor and Violation **2022**
Universe

Slowly Rotating Q-balls **2023**
European Physical Journal C

Mapping Excited Gauged Q-balls **2024**
To appear

ABSTRACT OF THE DISSERTATION

Exploring Aspects of Q-balls

By

Yahya Almumin

Doctor of Philosophy in Physics

University of California, Irvine, 2024

Professor Arvind Rajaraman, Co-Chair
Professor Michael Ratz, Co-Chair

Q-balls are an example of stable non-topological solitons that constitute of complex scalars emerging from $U(1)$-symmetric theories. In certain special potentials, complex scalars being bound together as Q-balls is energetically favorable compared to fragmenting into individual particles. In particle physics, Q-balls have theoretical and possibly phenomenological significance. Theoretically, it was demonstrated that these configurations could arise in supersymmetry, extra dimensions, and hidden sectors with QCD-like confinement. Phenomenologically, Q-balls are discussed as an interesting macroscopic dark matter candidate because of their stability and their possible formation in early universe.

In this dissertation, we explore theoretical aspects of Q-balls in order to provide a deeper analytical and numerical understanding of their properties in different set-ups. This is done by first studying excitation modes of global and gauged Q-balls in Chapter 2 and 3. Excited global Q-balls properties such as the size, charge and energy are described analytically in the thin-wall limit in Chapter 2. We show that despite the excited modes admitting a richer structure with multiple radii compared to the ground state, which is characterized by single radius, the properties of these modes are approximated by the leading order term of the radii. We also discuss the charge and energy of the excited states of global Q-balls, and

the stability of these modes. In Chapter 3, we build on the finding of the excited global Q-balls properties to approximate the excited gauged Q-balls properties by invoking a mapping relation that was derived in [4] for the ground state. We show the power of the mapping relation method to analytically describe a more complicated structure (gauged Q-ball) in terms of a simpler configuration (global Q-ball). The unique features of gauged Q-balls such as only allowing for a finite number of excitation modes and a maximal size per mode are derived in Chapter 3. Also, a discussion of the charge, energy and stability of the excited modes of gauged Q-balls is carried out in the same chapter.

In Chapter 4, we turn our attention to rotating Q-balls by discussing the possible existence of slowly rotating Q-balls. Traditionally, the angular momentum of rotating Q-ball is thought to be integer multiple of the charge. This implies that Q-balls with larger charge could not admit smaller angular momentum. We show that this conclusion follows as long as the integer multiple assumption is embedded in the ansatz. However, by perturbing a general Q-ball anstaz with angular momentum, a localized perturbative correction emerges. This hints to the existence of metastable slowly rotating Q-balls. We discuss the stability of these solutions as well.

Chapter 1

Introduction

1.1 Beyond The Standard Model

Particle physics is the branch of physics that is concerned with understanding the fundamental building blocks of the our universe and how the universe came about by applying the scientific method. *The Standard Model* (SM) of particle physics is the best theory that was discovered to describe the fundamental building blocks oof the universe. The SM divides particles in nature into two categories: fermions, which are the matter fields and bosons, which are the force carries. The "language" the SM invokes when describing the fundamental particles is *Quantum Field Theory* (QFT). QFT is the paradigm that describes the fabric of reality as quantized fields interacting with each other, and by studying the interaction of these fields we could predict the dynamics of our universe in the subatomic level. This picture of the universe proved extremely successful as it produced the Standard Model of particle physics that triumphed in the 20th century as the experimental evidence verified the accuracy of this description when it comes to visible matter.

Despite the remarkable success of the SM there are obvious shortcomings. While the SM was

able to characterize the ordinary matter, the Higgs, and three (electromagnetic, strong, and weak forces) out of the four forces in nature using QFT, the gravitational force could not be incorporated in the theory. Other deficiencies are within the SM itself as it does not provide an adequate explanation of the mass of the Higgs boson observed experimentally, which is know as the *hierarchy problem*. On the cosmological scale, ordinary matter does not seem to be sufficient to account for all the observable universe, and interestingly cosmological models predict that regular matter accounts for barely $\sim 4.9\%$ of the universe, and the rest of the universe is filled with *dark matter* and *dark energy* suggesting new physics beyond the SM might be necessary. The mystery of the universe does not reside exclusively in the invisible, but emerges in the visible matter as well. Existing in a universe with excess of matter to antimatter is quite puzzling when we consider they are thought to be identical in particle physics. This is known as *baryon asymmetry*, which is the puzzle of having an abundance of matter compared to antimatter, and mechanisms are needed to explain this imbalance. The SM baryogenesis can not account for the observable asymmetry. Therefore, alternative baryongensis mechanisms beyond the SM are proposed to explain the asymmetry. This is a non-exhaustive list of some of the problems that particle physics does not account for and probably requires physics beyond the SM.

One compelling method that offers a solution to the Higgs mass problem would be by imposing *Supersymmetry* (SUSY), which postulates a symmetry bosons and fermions. By introducing superpartners via SUSY, the Higgs mass will be protected against the large quantum corrections. This is possible because the loop corrections from the superpartners could cancel the corrections that come from the SM. However, no experimental evidence of these extra particles has been observed. Nontheless, SUSY is an interesting theoretical framework that extends the SM and intersects with particle physics problems, and has not been ruled out yet since their is still the possibility that SUSY resides in higher energy limits that we have not probed thus far.

The puzzle of the regular matter accounting for a small fraction of the content of the universe can be summed up as follows. For theoretical particle physics models of the universe to make sense i.e. match the observational data, we expect the existence of dark energy and dark matter to account for most of the content of the universe. More precisely, the universe expansion rate seems to be increasing over time and dark energy is postulated to be the driving force for this expansion. Dark matter, on the other hand, is proposed to account for multiple observational phenomena such as: galactic rotation curves and gravitational lensing. Galactic rotation curves is the observation that velocity of the stars and gases at the edge of the galaxies seems to be faster than expected if only ordinary visible matter is present. Gravitational lensing is the phenomenon where light bends due to the existence of some gravitational pull as predicted by Einstein's theory of relativity, and this phenomenon is observed in the sky in regions were visible matter is absent. Therefore, particle physicists suggest the existence of dark matter, which is a substance that leaves a gravitational imprint on the universe and lacks electromagnetic interaction impeding our ability to observe this form of matter, to account for these phenomena.

Thus, in spite of the success of the SM as theoretical in describing regular matter, there is an overwhelming evidence that a more complete theory beyond the Standard Model is needed to describe the full scope of the universe.

1.2 The Role of Q-balls in Particle Physics

After sketching a rough picture of the current state of particle physics, we turn our attention to a specific topic that has potential overlap with physics beyond the SM. Q-balls are stable non-topological solitons constituting of complex scalar carrying a $U(1)$ that have been proposed by Coleman in 1985 [5]. These configurations arise from $U(1)$ field theories as long as the potential satisfies Coleman conditions, which we will discuss thoroughly in Chapter 2.

Q-balls are configurations with finite energy, and it is energetically more favourable for the complex scalars to be bound together in single Q-ball state instead of decaying into individual particle or to smaller Q-balls. The charge of Q-balls, if normalized properly, corresponds to the number of complex scalars that makes up the non-topological soliton configuration.

As explained in the previous section, field theory is the underlying framework that seems to describe the fundamental building blocks of the universe. Thus, from a purely theoretical point of view, studying Q-balls is well-motivated as these objects arise naturally in field theory with the appropriate potential. Q-balls emerge from various particle physics models such as supersymmetry [6, 7], extra dimensions [8, 9], and hidden sectors with QCD-like confinement [10, 11]. Also, they have been discussed in the context of baryon asymmetry [7, 12] and observable gravitational wave [13, 14].

However, the significance of Q-balls when it comes to phenomenology stems from their possible connection to dark matter. Despite the invisible nature of dark matter due to their lack of interaction with light, there is a plethora of models that try to predict the nature of these objects based on their observed impact on the universe. Examples of famous dark matter candidates are *Weakly Interacting Massive Particles* (WIMPs) and *axions*. WIMPs are thought to be particles that interact with regular matter exclusively through the gravitational force and weak force. On the other hand, axions were hypothesised to address the *strong CP problem* where quantum chromodynamics permits the violation of charge conjugation parity (CP) symmetry but experimentally the strong force seems to preserve the CP symmetry. Nonetheless, the weak coupling between axioms and the SM particles make these hypothetical particles interesting dark matter candidates. A number experiments are set-up globally to search for these candidates like XENONS, EDELWEISS, and CDMS for WIMPS, and ADMX for axions. Unfortunately, however, no conclusive experimental evidence was discovered of these hypothetical particles so far. This opens the way to study other exotic models that attempt to describe dark matter. Macroscopic dark matter may represent a

subset of models, which postulate that dark matter constitutes of composite objects that are lighter than ultra heavy dark matter. An example of a macroscopic dark matter model that was rules out is hot quarks nuggets. However, the possible formation of Q-balls in early universe [15, 16, 13, 17, 18] coupled with their stability [5] and size make these configurations excellent macroscopic dark matter candidates [19, 20, 21, 22, 23, 24].

Therefore, Q-balls have theoretical significance as they represent a class of stable solitonic solutions to field theories with non-topological charge. Nevertheless, their relevance extends beyond the theoretical discussion as these non-topological solitons intersect with various phenomenological particle physics questions.

1.3 Motivation

While considerable strides have been made to understand Q-balls, further analysis is needed to produce a complete theoretical understanding of the full Q-ball space. As we pointed out earlier, Q-balls are intriguing macroscopic dark matter candidate, and in order to build testable phenomenological models theoretical investigation is necessary to hunt for them. Thus, the purpose behind this dissertation is to explore theoretical aspects about Q-balls to pave the way for model building in the near future.

Q-balls are solutions of non-linear differential equations and their profiles and properties are dependent on the potential that gives rise to these configurations. Usually the profiles and properties of the non-topological solitons are solved numerically since only a subset of these differential equations can be solved analytically [25]. Some potentials have analytical solutions but they are usually unphysical [26, 27, 28, 29].

A potential that produces Q-balls that is analytically solvable is the sextic potential. An analytical analysis of the ground state of Q-balls arising in sextic have been produced in

these papers [1, 4, 30]. However, in order to have a complete understanding of the full space of the Q-ball solutions, it is necessary to explore the excited states as well. As discussed in the previous section, Q-balls analysis significance extends beyond the theoretical scope. Excited states [31, 32] will inevitably play a role in the formation and scattering of global Q-balls [33] despite their instability. Also, if these excited states are long-lived due to having small energy gap between these states and the ground, phenomenological implications could be relevant. Charge-swapping Q-balls is an example of excited Q-balls that were shown to be qusai-stable [34, 35, 36, 37]. Thus, analytically characterizing properties of radial excitation of (global/gauged) Q-balls is crucial theoretically and phenomenologically.

Another aspect of Q-balls would be rotation. A standard assumption when dealing with rotating Q-balls is that the angular momentum is thought to be an integer multiple of the charge of the Q-ball [31, 38, 39, 40, 41, 42] and (the closely related boson stars [43, 44, 45, 46, 47, 48, 49, 50, 51, 52, 53, 54, 55]). However, if we think of Q-balls as large classical objects, one could imagine the angular momentum to have an arbitrarily small value. Since it is assumed that miniclusters with angular momentum could collapse into Q-balls, a different phenomenological picture would emerge depending on the allowed values of the angular momentum of rotating Q-balls. Therefore, investigating the angular momentum assumption is pivotal to better understand the properties and formation of rotating Q-balls.

In the following chapters of the dissertation we explore these problems in great depth. Chapter 2 is concerned with characterizing excited global Q-balls properties in a sextic potential. This is done by deriving relations between the physical characteristics of the excited states and the parameter κ. In Chapter 3, we investigated excited gauged Q-balls properties using a mapping relation with the global case. Solving the non-linear differential equations of gauged Q-balls is notably difficult analytically and numerically. However, as shown for the ground state of gauged Q-balls in Ref. [4], by mapping the ground states of the global and gauged Q-balls, the properties of the gauged Q-ball could be solved in terms of the

simpler global case. We extend this method to excited gauged Q-balls to explore the properties of the excitation modes. We shift gears in Chapter 4 and Appendix A, and discuss rotating Q-balls. In this chapter we propose a general ansatz for rotating Q-balls without the constraining the angular momentum value to be integer multiple of the charge. Even though the solutions we found are classically metastable, the finding suggests slowly rotating Q-balls are theoretically viable and might be significant phenomenologically. We conclude the dissertation in Chapter 5.

Chapter 2

Excited Global Q-balls

This chapter is heavily based on work previously published in collaboration with Julian Heeck, Arvind Rajaraman, and Christopher B. Verhaaren [2].

2.1 Introduction

The Q-ball ground-state configuration has the lowest energy for a given $U(1)$ charge, rendering it stable [5]. Exact analytical solutions can only be obtained for special—typically unphysical—potentials, other cases have to be approached numerically or via analytic approximations. The latter case is particularly fruitful for large Q-balls, with the large radius acting as a good expansion parameter. In Ref. [1], excellent analytic approximations for Q-balls in a sextic potential were recently provided, which essentially eliminate the need to solve the differential equations numerically. This paves the way for further phenomenological studies to include Q-balls states accurately without continually solving the nonlinear systems that define them.

Spherically symmetric ground-state configurations of the form $\phi(\vec{x},t) = \tilde{\phi}(|\vec{x}|)e^{\mathrm{i}\omega t}$ [5] are

typically the simplest solutions and those of most interest for phenomenological studies, given their stability. Nevertheless, the study of unstable excited states is useful and necessary because Q-ball formation and scattering will generally also produce excited states that eventually relax into the ground state [15, 33, 16, 13, 17, 18]. The details of the excitation spectrum are therefore important, e.g. for Q-ball dark matter, just like the study of excited nuclei and atoms. In the early universe, the scalars ϕ and Q-balls are expected to be in thermal equilibrium [56, 57, 58]; excited states will then be in equilibrium as well, with their abundance suppressed by their larger mass. It is therefore crucial to know the mass gap or spectrum of Q-balls of fixed charge Q to ascertain their relevance in the cosmological evolution. Similarly, any scattering of or off Q-balls generically produces excited states unless kinematically forbidden due to a large mass gap. Furthermore, the lifetimes of excited states could be long if the available phase space is suppressed: on general grounds, the lifetime of an excited state will scale inversely with some power of the energy gap ΔE to the ground state due to the reduced phase space; for a compressed excitation spectrum, the lifetimes of the excited states could hence be large enough to be of phenomenological interest [33].

Building on the ground-state work of Ref. [1], we therefore study excited Q-ball states, providing useful analytical approximations to the exact solutions, as shown by our comparison to the numerical data. Excited Q-balls with angular momentum $J \neq 0$, have been discussed in Refs. [31, 44] and shown to have energies that exceed the non-rotating ground-state energy by at least $\sim 20\%$ for the same charge Q. These initial studies give a reasonable idea of the Q-ball spectrum in terms of angular momentum, albeit only for a small region in parameter space. In addition to these rotational excitations, Q-balls exhibit spherically symmetric *radial* excitations with vanishing angular momentum, discovered in Refs. [59, 31]. Numerical solutions for the first 23 radial excitations for a fixed frequency ω have been computed and discussed in Ref. [32].[1] Because ω was fixed, all these excitations have different charges Q, so they cannot be interpreted as physical excitations of each other or a specific ground state

[1]The excited states of *gauged* Q-balls for the sextic potential are explored in Ref. [60].

soliton. In fact, to the best of our knowledge, no study of the radial excitation spectrum for a fixed Q exists in the literature. It has, therefore, not yet been established whether the lowest-lying Q-ball excitation is radial or rotational. Building upon and generalizing aspects of previous work, our efforts below are able to characterize all radial excited states for the complete family of sextic potentials and all phases, providing the full radial spectrum. Despite our analysis being performed for one particular scalar potential, we expect our results to be valuable more generally and adaptable to other potentials.

In the following section we review the theory of ground state Q-balls to establish notation, conventions, and the definitions of physical characteristics like charge and energy. We also review the different types of stability these solitons may exhibit. Section 2.3 motivates an analytic form for excited state Q-balls and methods to fully characterize them in terms of the potential parameters. Approximations to the physical characteristics of the excited states are obtained in Sec. 2.4 as well as a discussion of their stability and possible decay channels. In Sec. 2.5 we outline how our results are expected to generalize to other potentials. We conclude in Sec. 2.6.

2.2 Review Global Q-Balls Ground-State

We recount the well-known case of ground-state Q-balls to establish our notation, following closely Ref. [1]. The Lagrangian for the complex scalar ϕ is simply

$$\mathcal{L} = |\partial_\mu \phi|^2 - U(|\phi|), \tag{2.1}$$

with a $U(1)$ invariant potential U that has to fulfill a number of conditions to support Q-ball solutions. Since we do not want to break the $U(1)$ symmetry, we require $\langle\phi\rangle = 0$ in the vacuum; we normalize the potential energy to zero in the vacuum by setting $U(0) = 0$ and

enforce that the vacuum is a stable minimum of the potential by demanding

$$\left.\frac{\mathrm{d}U}{\mathrm{d}|\phi|}\right|_{\phi=0} = 0\,, \qquad \left.\frac{\mathrm{d}^2U}{\mathrm{d}\phi\,\mathrm{d}\phi^*}\right|_{\phi=0} = m_\phi^2 > 0\,, \tag{2.2}$$

where m_ϕ is the mass of the complex scalar. Coleman [5] showed that nontopological solitons, Q-balls, exist when the function $U(|\phi|)/|\phi|^2$ has a minimum at $|\phi| = \phi_0/\sqrt{2} > 0$[2] such that

$$0 \leq \sqrt{\frac{2U(\phi_0/\sqrt{2})}{\phi_0^2}} \equiv \omega_0 < m_\phi\,. \tag{2.3}$$

In this case, the spherically symmetric Q-ball solutions take the form

$$\phi(x^\mu) = \frac{\phi_0}{\sqrt{2}} f(r) e^{\mathrm{i}\omega t}\,, \tag{2.4}$$

where $f(r)$ is a dimensionless function of the radius r and ω is a constant internal frequency that is restricted to the region $\omega \in (\omega_0, m_\phi)$. Switching to a dimensionless radial coordinate ρ defined by

$$\rho = r\sqrt{m_\phi^2 - \omega_0^2}\,, \tag{2.5}$$

we end up with the effective Lagrangian for $f(\rho)$

$$L = \frac{4\pi\phi_0^2}{\sqrt{m_\phi^2 - \omega_0^2}} \int \mathrm{d}\rho\; \rho^2 \left[-\frac{1}{2} f'^2 + V(f)\right], \tag{2.6}$$

[2]One can in fact consider Q-balls with only a thick-wall limit [61, 62] in certain potentials. In this case ϕ_0 is not defined.

where a prime denotes a derivative with respect to ρ and the effective potential $V(f)$ is defined via

$$V(f) = \frac{1}{m_\phi^2 - \omega_0^2} \left(\frac{\omega^2}{2} f^2 - \frac{U(f\phi_0/\sqrt{2})}{\phi_0^2} \right). \tag{2.7}$$

The Euler-Lagrange equation

$$f'' + \frac{2}{\rho} f' + \frac{\mathrm{d}V}{\mathrm{d}f} = 0\,, \tag{2.8}$$

is then equivalent to a particle of position f moving in the potential $V(f)$ while subject to friction, ρ corresponding to the time coordinate in this analogy [5]. The boundary conditions are $f'(0) = 0$ and $f(\rho \to \infty) = 0$ in order to obtain localized solutions. The charge Q and energy E of the Q-ball are defined as

$$\begin{aligned} Q &= i \int \mathrm{d}^3x \left(\phi^* \partial^0 \phi - \dot{\phi}^* \partial^0 \phi \right) , \\ E &= \int \mathrm{d}^3x \left[|\partial_\mu \phi|^2 + U(|\phi|^2) \right] , \end{aligned} \tag{2.9}$$

and the integrals are written in our re-definition as

$$\begin{aligned} Q &= i \int \mathrm{d}^3x \left(\phi^* \partial^0 \phi - \dot{\phi}^* \partial^0 \phi \right) = \frac{4\pi\omega\phi_0^2}{(m_\phi^2 - \omega_0^2)^{3/2}} \int \mathrm{d}\rho\, \rho^2 f^2\,, \\ E &= \int \mathrm{d}^3x \left[|\partial_\mu \phi|^2 + U(|\phi|^2) \right] = \omega Q + \frac{4\pi\phi_0^2}{3\sqrt{m_\phi^2 - \omega_0^2}} \int \mathrm{d}\rho\, \rho^2 f'^2\,, \end{aligned} \tag{2.10}$$

which satisfy the differential equation $\mathrm{d}E/\mathrm{d}\omega = \omega \mathrm{d}Q/\mathrm{d}\omega$ [59, 63, 1].

To be more concrete, let us consider the sextic potential

$$U(\phi) = m_\phi^2 |\phi|^2 - \beta |\phi|^4 + \frac{\xi}{m_\phi^2} |\phi|^6\,, \tag{2.11}$$

which is non-renormalizable but can easily be UV-completed by introducing heavier particles.

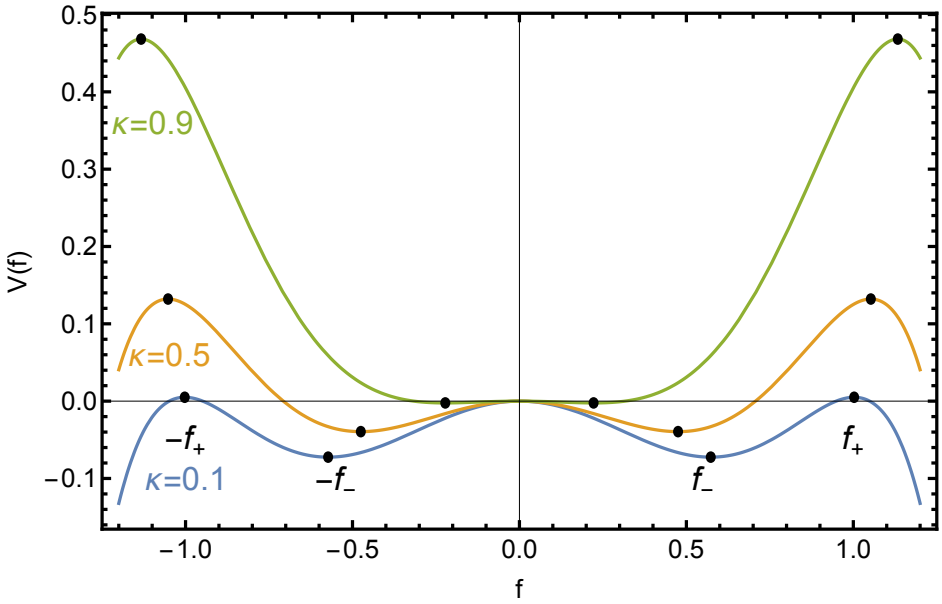

Figure 2.1: Potential $V(f)$ for $\kappa = 0.1$ (blue), $\kappa = 0.5$ (tan), and $\kappa = 0.9$ (green). The extrema $(\pm)f_\pm$ are shown as black dots.

Replacing the parameters β and ξ by ϕ_0 and ω_0, this potential leads to the function V

$$V(f) = \frac{1}{2} f^2 \left[\kappa^2 - (1 - f^2)^2\right], \qquad \text{with} \qquad \kappa^2 \equiv \frac{\omega^2 - \omega_0^2}{m_\phi^2 - \omega_0^2}, \tag{2.12}$$

where $\kappa \in (0, 1)$ [1]. The potential has extrema at $f = 0$ and

$$f_\pm^2 = \frac{1}{3}\left(2 \pm \sqrt{1 + 3\kappa^2}\right). \tag{2.13}$$

As shown in Fig. 2.1, the $\pm f_+$ are maxima while $\pm f_-$ are local minima.

The differential equation (2.8) depends only on the parameter κ, which must therefore determine the radius of the Q-ball. For ground-state solutions we demand $f(\rho)$ to be a monotonic function and define the radius R_0^* through $f''(\rho = R_0^*) = 0$. In the limit of large R_0^* or small κ, the friction term $2f'/\rho$ in Eq. (2.8) becomes negligible, allowing us to find the approximate

profile $f(\rho)$ in the form of the so-called transition function

$$f_T(\rho) = \frac{1}{\sqrt{1+2e^{2(\rho-R_0^*)}}}\,, \tag{2.14}$$

which becomes an exact solution in the limit $R_0^* \to \infty$ [1]. For small κ, this transition from $f = f_+ \simeq 1$ to $f = 0$ reduces the energy by $1/(2R_0^*)$ due to friction. The total energy loss must be the difference between the initial maximum, with energy given at leading order in κ by

$$V(f_+) = \frac{2+\sqrt{1+3\kappa^2}}{27}\left(\sqrt{1+3\kappa^2}-1+3\kappa^2\right) = \frac{\kappa^2}{2} + \mathcal{O}(\kappa^4)\,, \tag{2.15}$$

and the final maximum at $V(0) = 0$. This implies that to leading order in small κ:

$$\frac{1}{2R_0^*} = \frac{\kappa^2}{2} \quad \Rightarrow \quad R_0^* = \frac{1}{\kappa^2}\,. \tag{2.16}$$

This relation between radius and small κ is a good approximation for all stable ground-state solutions [1]. With these predictions for the radius and profile we can also obtain analytic expression for energy and charge via Eq. (2.10).

2.2.1 Ground State Stability

Discussions of stability regarding Q-ball ground states are often divided into three categories: absolute stability, classical stability, and stability to fission [64]. The absolute stability criterion is the simplest: it is the requirement that the soliton solution of charge Q have a lower energy than Q free scalar particles. In other words, the Q-ball energy E must satisfy $E < m_\phi Q$. This is referred to as absolute stability because it is stable against both classical and quantum effects [63]. In our sextic potential, ground-state solutions are absolutely stable

for $\kappa \lesssim 0.84$ [1], so in particular in the thin-wall regime $\kappa \ll 1$.

Classical stability is taken to mean that the soliton is stable against perturbations; if perturbations can grow without bound, then the solution is said to be unstable. It has been shown that when

$$\frac{\omega}{Q}\frac{\mathrm{d}Q}{\mathrm{d}\omega} \leq 0\,, \tag{2.17}$$

the corresponding Q-ball solutions are classically stable [59, 63]. We are free to choose both $\omega > 0$ and $Q > 0$, so the more significant condition for that choice is

$$\frac{\mathrm{d}Q}{\mathrm{d}\omega} \leq 0\,. \tag{2.18}$$

In the sextic potential, this requirement is automatically satisfied in the absolutely-stable region with $\kappa \lesssim 0.84$ and hence a weaker criterion. It is worth noting that the derivation of Eq. (2.18) also demonstrates that the radial profile for these classically stable ground-state solitons have no nodes [59, 5, 63].

The final stability criterion is related to a soliton breaking up into smaller solitons and free particles, something like the fission of a nucleus. It was argued in [63] that the condition in (2.18) also prevents Q-ball fission. This can be seen from the following argument given in [65]. Using $\mathrm{d}E/\mathrm{d}Q = \omega$, we can write

$$\frac{\mathrm{d}\omega}{\mathrm{d}Q} = \frac{\mathrm{d}}{\mathrm{d}Q}\frac{\mathrm{d}E}{\mathrm{d}Q} = \frac{\mathrm{d}^2E}{\mathrm{d}Q^2}\,. \tag{2.19}$$

This means that when $\frac{\mathrm{d}Q}{\mathrm{d}\omega} < 0$ it follows that

$$\frac{\mathrm{d}^2 E}{\mathrm{d}Q^2} < 0 \ . \tag{2.20}$$

Consider the possible fission of a Q-ball of charge $Q_1 + Q_2$ that breaks into two solitons of charge Q_1 and Q_2, respectively. We integrate the inequality in (2.20) from some intermediate charge Q_i up to $Q_i + Q_2$:

$$\int_{Q_i}^{Q_i+Q_2} \mathrm{d}Q \, \frac{\mathrm{d}^2 E}{\mathrm{d}Q^2} < 0 \ \Rightarrow \ \left.\frac{\mathrm{d}E}{\mathrm{d}Q}\right|_{Q_i+Q_2} < \left.\frac{\mathrm{d}E}{\mathrm{d}Q}\right|_{Q_i} \ . \tag{2.21}$$

We then integrate this resulting inequality with respect to the intermediate charge Q_i from 0 to Q_1. Because $E(0) = 0$, this leads to

$$E(Q_1 + Q_2) < E(Q_2) + E(Q_1) \ , \tag{2.22}$$

which means that fission is energetically forbidden if Eq. (2.18) is satisfied.

2.3 Excited State Solutions

Heretofore we have assumed that the rolling particle always has $f \geq 0$. However, one can imagine the particle beginning from rest and then rolling down the hill in positive f, over the maximum at $f = 0$, up the hill in negative f, and back toward rest at $f = 0$. Such a trajectory satisfies the Q-ball boundary conditions and leads to a localized solution. The

corresponding solitons are said to belong to the first excited state of some Q-ball [31, 32], for reasons which are made clear below. More generally, the particle can roll back and forth several times before settling down at $f = 0$, which defines an entire tower of excited states. We label the excited states by the number N of transitions through $f = 0$, with $N = 0$ being the $f \geq 0$ ground state.

The only way to enable the particle to roll a longer distance is for it to begin with larger potential energy. Thus, for a fixed κ, energy conservation suggests that the particle's initial position $f(0)$ moves closer to the maximum f_+ for increasing N. Starting closer to the maximum implies the particle's velocity is nearly zero for a longer time during which the friction term decreases. When larger scale motion eventually begins, the friction has deceased sufficiently for the particle to complete the larger number of back-and-forth transitions before coming to rest. In short, by delaying the onset of motion in transition toward $f = 0$ the particle loses less energy to friction. Qualitatively, this shows that there is an infinite tower of excited states for a given κ with each higher N trajectory beginning slightly closer to the maximum f_+. It also suggests that the radius of the Q-ball (the 'time' of the first transition) grows with N for large enough N, which is confirmed by the numerical results that follow.

Notice that for a fixed κ, the $N = 0$ and $N > 0$ states do not have the same Q [32], so they should not be regarded as excitations of each other. This follows from the rolling particle analogy upon realizing that the $N > 0$ states necessarily start off closer to f_+ in order to have sufficient energy for their additional transitions, which results in a larger integral $\int \mathrm{d}\rho\, \rho^2 f^2$ and thus a larger Q due to Eq. (2.10). In addition, stable Q-balls require $\mathrm{d}Q/\mathrm{d}\omega < 0$ [64], or $\mathrm{d}Q/\mathrm{d}\kappa < 0$ in our notation, so Q *decreases* with increasing κ. Therefore, to have the $N = 1$ soliton's Q match a $N = 0$ soliton Q, the κ of the excited state must be *larger* than the ground state κ. Generally, exciting a Q-ball from N to $N + 1$ requires an increase in κ or ω to keep Q the same. The energy (Eq. (2.10)) of the excited state for a fixed Q then unavoidably increases, both due to the larger ω and because the surface integral $\int \mathrm{d}\rho\, \rho^2 (f')^2$

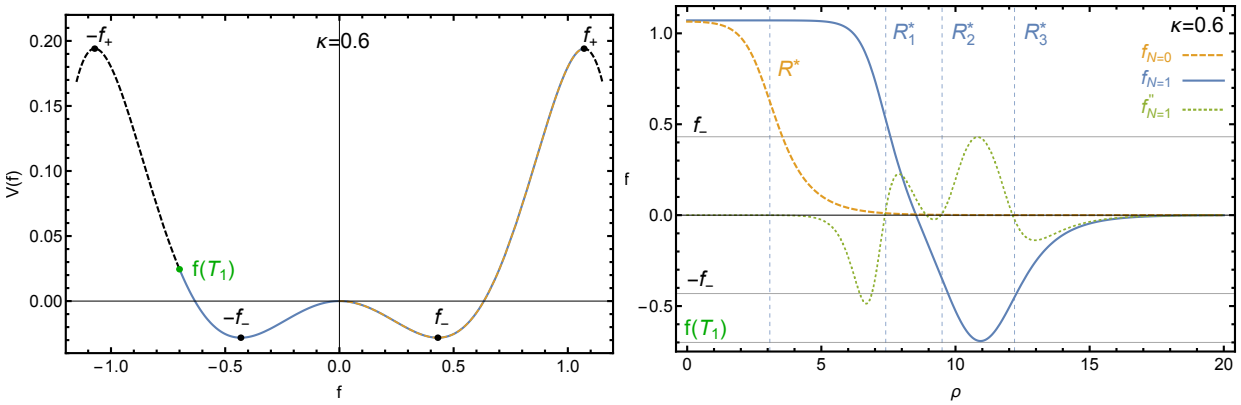

Figure 2.2: Effective potential $V(f)$ (left) and $N = 1$ excited state profile $f(\rho)$ (right). The solid line in the potential denotes the path along which the particle rolls. The locations of the relevant extrema of $V(f)$, $f_\pm$ are denoted in each plot, as is the location of the turning point $f(T_1)$.

increases with every back-and-forth transition, justifying the terminology that each larger N soliton is an excited state of an $N = 0$ Q-ball.

2.3.1 Profiles

Most of the characteristics of excited-state trajectories may be understood by considering the $N = 1$ example shown in Fig. 2.2. Even for this $\kappa = 0.6$ example (which is not close to the $\kappa \to 0$ thin-wall limit) the particle begins at rest near the local maximum at f_+. After remaining for some time near the maximum, it transitions quickly down the potential hill. In fact, it is more useful to consider the particle as having approximately three transitions. The first is similar to the ground state Q-ball (the dashed tan line in the figure), rolling from f_+ to $f = 0$. Instead of stopping, however, it then transitions uphill in negative f. The particle has lost energy due to friction along its way, so the turning point $f(T_1)$ is well below the maximum at $-f_+$. The particle finally transitions back down from the turning point and comes to rest at on the maximum at $f = 0$. The profile in physical space that corresponds to this particle trajectory is shown as the solid blue line in the right panel of Fig. 2.2.

The $N = 0$ (dashed tan) and $N = 1$ (solid blue) profiles on the right side of Fig. 2.2 illustrate several points. First, we see that the initial value $f(0)$ of the first excited state profile is larger

than the $f(0)$ for the ground state, as expected. Consequently, the excited state remains near the f_+ maximum until a larger ρ, allowing it to lose much less energy as it rolls. For the ground state there is only one point with $f'' = 0$, which defines the radius R_0^*. However, for the excited state there are four points where $f'' = 0$ (small dashed green). Three of these are near to where $f \approx \pm f_-$, and we have labeled these $R_{1,1}^*$, $R_{1,2}^*$, and $R_{1,3}^*$. The remaining zero of f'' is near to $f \approx 0$. One can see that the f'' roots associated with $f = 0$ and R_2^* are somewhat marginal, and indeed as κ increases, these two roots no longer have real solutions.

Describing the motion as three transitions—each with a defining radius at which $f'' = 0$ but $f \neq 0$—allows us to make an ansatz for f as the product of transition functions of the form given in Eq. (2.14):

$$f_{N=1} = \left[f_T(\rho, R_{1,1}^*) - f_T(-\rho, -R_{1,2}^*)\right] f_T(\rho, R_{1,3}^*)\,, \tag{2.23}$$

where $R_{1,1}^* < R_{1,2}^* < R_{1,3}^*$. Just like the transition profile of the ground state, this is only expected to be a reasonable form for large radii or small κ. In Fig. 2.3, we show the exact numerical profiles $f_{N=1}$ for $\kappa = 0.4$ and 0.1 together with the above transition-function ansatz, fitting the three radii to the numerical data. For small κ, the agreement is remarkable and illustrates that the $N = 1$ profile can be completely specified by the three radii $\{R_{1,1}, R_{1,2}, R_{1,3}\}$. At larger κ, this ansatz becomes increasingly inadequate—just like in the ground-state case. We return to the large κ regime in subsection 2.3.3, for now we focus on small κ.

The extension of Eq. (2.23) for the Nth excited state is simply

$$f_N = \left[f_T(\rho, R_{N,1}^*) - f_T(-\rho, -R_{N,2}^*)\right] \cdots \left[f_T(\rho, R_{N,2N-1}^*) - f_T(-\rho, -R_{N,2N}^*)\right] f_T(\rho, R_{N,2N+1}^*)\,, \tag{2.24}$$

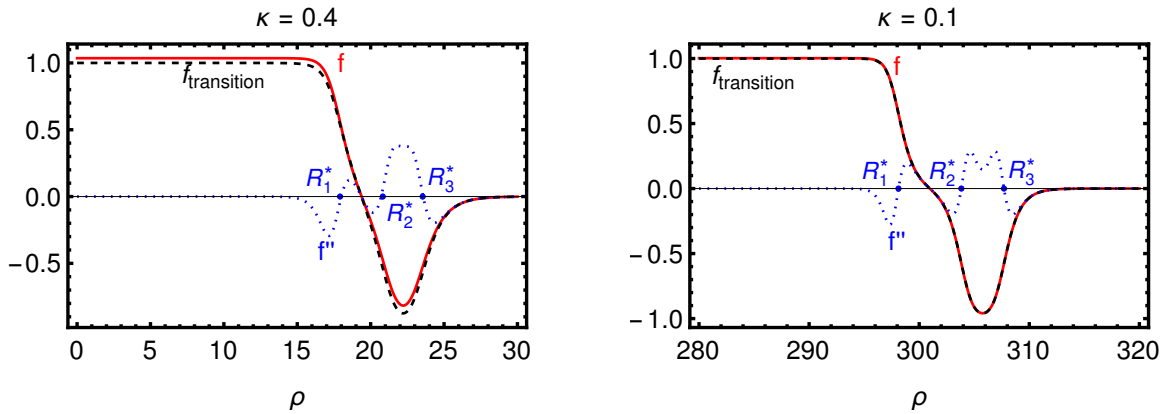

Figure 2.3: Numerical profiles $f(\rho)$ in red for $\kappa = 0.4$ (left) and $\kappa = 0.1$ (right). Also shown in dashed black is the analytic approximation $f_{\text{transition}}$ from Eq. (2.23); the latter depends on the three radii R_j^* defined by $f''(R_j^*) = 0$ (not the one at $f = 0$). The agreement between numerical and transition profile becomes better for small κ.

specified by $2N + 1$ radii $R^*_{N,n}$, $n = 1, 2, 3, \ldots, 2N + 1$. The agreement with the numerical profiles is similar to Fig. (2.3) and generally excellent for small κ. Though the numerical results necessarily assume a particular potential, the form of the excited state profile in terms of transition functions can be applied to any potential.

2.3.2 Thin-Wall Limit

The product of transition functions in Eq. (2.24) is an empirically successful approximation for the excited-state profiles at small κ. It requires $2N+1$ radii $R^*_{N,n}$, $n = 1, 2, 3, \ldots, 2N+1$, as input, which can only depend on the small parameter κ and necessarily diverge in the small κ limit just like in the ground-state case. In this section, we derive the relations $R^*_{N,n}(\kappa)$ for small κ.

For the ground state, a small κ transition reduced the particle energy by $1/(2R_0^*)$ [1]. The first excited state with its three transitions is then expected to lose an energy of approximately $3/(2R_1^*)$ due to friction. The total energy loss must be the difference between the initial maximum, with energy given at leading order in κ by Eq. (2.15), and final maximum at

$V(0) = 0$. This implies that to leading order in small κ

$$\frac{3}{2R_1^*} = \frac{\kappa^2}{2} \;\Rightarrow\; R_1^* = \frac{3}{\kappa^2}\,. \tag{2.25}$$

We therefore expect all three radii of the first excited state, $R_{1,n}^*$, to be around $3/\kappa^2$, with only small differences $\Delta_n \equiv R_{1,n}^* - R_{1,n-1}^*$ that are subleading in small κ. Similarly, the general Nth excited state is expected to have radii that are clustered around

$$R_{N,n}^* = \frac{2N+1}{\kappa^2}\,, \tag{2.26}$$

further split up by terms that are subleading in small κ, to be discussed next.

To estimate the $2N+1$ individual radii beyond Eq. (2.26) we need to determining the radial distance between them. In the thin-wall limit we may neglect friction. Then, the "time" it takes for a particle to roll from one point on the effective potential to another is given by

$$\rho_2 - \rho_1 = \int_{f_1}^{f_2} \frac{\mathrm{d}f}{\sqrt{2\mathcal{E} - 2V(f)}}\,, \tag{2.27}$$

where $f(\rho_i) = f_i$ and

$$\mathcal{E} = \frac{1}{2}f'^2 + V(f)\,, \tag{2.28}$$

is the conserved energy of the particle [1]. In this same frictionless limit the particle's

equation of motion is

$$f'' = -\frac{\mathrm{d}V}{\mathrm{d}f}\,. \tag{2.29}$$

This means the values of f for which $f'' = 0$ (which define the radii) are exactly the extrema of $V(f)$. More particularly, as is clear from Fig. 2.2, we are interested only in the extrema that occur when $f \neq 0$. Then, to find the distance between the radii, we consider two types of trajectories. Those that pass through $f = 0$, such as from $f = f_-$ to $f = -f_-$, and those that run from the potential minimum to a turning point, such as from $f = -f_-$ up the potential hill to the turning point $f(T_i)$ and then back to $f = -f_-$.

In the thin-wall (or small κ) limit, only a small range of $f \sim f_+$ correspond to $V(f) > 0$. As the particle loses energy to friction and must end at $V(0) = 0$, the particle's initial location must be in this small region $f \lesssim f_+$. This also ensures that it does not begin to transition until the friction is largely absent so that the energy loss is small. Thus, the value of $\mathcal{E}$ is also small, with f beginning on the potential with $f' = 0$. The be more precise,

$$\mathcal{E} \approx V(f_+) = \frac{\kappa^2}{2} + \mathcal{O}(\kappa^4)\,. \tag{2.30}$$

This means that we can expand the "time" integral as

$$\begin{aligned}&\int \mathrm{d}f \left[\frac{1}{f(1-f^2)} + \frac{f^2\kappa^2 - 2\mathcal{E}}{2f^3(1-f^2)^3} + \mathcal{O}(\kappa^4)\right] \\ &= \frac{1}{2}\left(1 + \frac{1}{2}\kappa^2 + 3\mathcal{E}\right)\ln\frac{f^2}{1-f^2} + \frac{3-2f^2}{8(1-f^2)^2}\kappa^2 - \frac{2-9f^2+6f^4}{4f^2(1-f^2)^2}\mathcal{E} + \mathcal{O}(\kappa^4)\,.\end{aligned} \tag{2.31}$$

It remains to specify the limits of integration. We first consider the trajectories that change the sign of f. The relevant interval is $-f_-$ to f_-, which provides estimates for $R^*_{N,\mathrm{even}} - R^*_{N,\mathrm{odd}}$.

However, as Eq. (2.31) is a function of f^2 and the limits of integration are even, it seems that the integral vanishes. The subtlety is the singularity at $f = 0$.

Our approximation is not valid when $f \approx 0$. That is, when $f^2 \sim \kappa^2$ the expansion in Eq. (2.31) breaks down. But, in this regime the potential can be well approximated by the quadratic term

$$V(f) \approx -\frac{1}{2}(1-\kappa^2)f^2 + \mathcal{O}(f^4)\,. \tag{2.32}$$

We can then integrate

$$\int \frac{\mathrm{d}f}{\sqrt{2\mathcal{E} + (1-\kappa^2)f^2}} = \frac{1}{\sqrt{1-\kappa^2}} \ln\left[f(1-\kappa^2) + \sqrt{1-\kappa^2}\sqrt{2\mathcal{E} + f^2(1-\kappa^2)}\right]. \tag{2.33}$$

We assume that these two regimes are joined at some value $f = f_j$. We need $f_j > \kappa$, so that the expansion for $f > f_j$ is justified. A consistent choice is $f_j = \sqrt{\kappa}$. Then we find

$$\begin{aligned}\int_0^{f_j} \frac{\mathrm{d}f}{\sqrt{2\mathcal{E} + (1-\kappa^2)f^2}} &= \frac{1}{\sqrt{1-\kappa^2}} \ln \frac{f_j\sqrt{1-\kappa^2} + \sqrt{2\mathcal{E} + f_j^2(1-\kappa^2)}}{\sqrt{2\mathcal{E}}} \\ &= \frac{1}{2}\ln\frac{2f_j^2}{\mathcal{E}} + \frac{\mathcal{E}}{2f_j^2} + \mathcal{O}(\kappa^2)\,.\end{aligned} \tag{2.34}$$

The other part of the integration is from f_j to f_- and is found to be

$$\int_{f_j}^{f_-} \mathrm{d}f \left[\frac{1}{f(1-f^2)} + \frac{f^2\kappa^2 - 2\mathcal{E}}{2f^3(1-f^2)^3} + \mathcal{O}(\kappa^4)\right] = \frac{1}{2}\ln\frac{f_-^2(1-f_j^2)}{f_j^2(1-f_-^2)} - \frac{\mathcal{E}}{2f_j^2} + \mathcal{O}(\kappa^2)\,. \tag{2.35}$$

Note that when these terms are combined that the term linear in $\mathcal{E}$ (and also in κ) cancels.

The leading result is

$$\int_0^{f_-} \frac{\mathrm{d}f}{\sqrt{2\mathcal{E} - 2V(f)}} = \frac{1}{2} \ln \frac{2f_-^2}{\mathcal{E}(1-f_-^2)} + \mathcal{O}(\kappa^2)\,. \tag{2.36}$$

By multiplying by two, we obtain the full trajectory from $-f_-$ to f_- and so

$$\Delta_{\text{even}} = \ln \frac{2f_-^2}{\mathcal{E}(1-f_-^2)}\,, \tag{2.37}$$

is our leading order estimate of $R^*_{N,\text{even}} - R^*_{N,\text{odd}}$.

Before this can be used to estimate excited state radii we need to determine $\mathcal{E}$. The initial energy of the particle rolling the potential is taken to be approximately $V(f_+)$. The particle loses energy until is stops at $V(0) = 0$. We estimate the energy loss by dividing the total energy equally among all the transitions, which for the Nth excited state is $2N+1$ transitions. The energy at the beginning of the nth transition is given by

$$\mathcal{E}_n = V(f_+)\frac{2N+2-n}{2N+1} \approx \frac{\kappa^2}{2}\frac{2N+2-n}{2N+1}\,, \tag{2.38}$$

where in the last expression we use the leading order in κ result.

Finally, to determine Δ_{odd} we must estimate the "time" it takes the particle to go from the minimum of the potential up to a turning point and back. This is equivalent to twice the integral from $-f_-$ up to the turning point f_T of the particle. This turning point is

determined by the equation

$$V(f_T) = \frac{f_T^2}{2}\left[\kappa^2 - \left(1 - f_T^2\right)^2\right] = \mathcal{E}_n\,. \tag{2.39}$$

Because of the symmetry of the potential, we consider the equivalent trajectory with $f > 0$. In the $\kappa \to 0$ limit $f_T \lesssim 1$, so the $1 - f^2$ terms in the denominator of Eq. (2.31) can invalidate the expansion. Since $f_T \to 1$ as $\kappa \to 0$ we parameterize the turning point location as

$$f_T = 1 - T\kappa\,. \tag{2.40}$$

To leading order in κ Eq. (2.39) becomes

$$\frac{1}{2}(1 - T^2)\kappa^2 = \frac{\kappa^2}{2}\frac{2N + 2 - n}{2N + 1}\,, \tag{2.41}$$

which implies that

$$T = \sqrt{\frac{n-1}{2N+1}}\,. \tag{2.42}$$

Note here that while n labels the transition, only odd n's larger than one are actually associated with turning points. So, we label the mth turning point, with $n = 2m + 1$, as

$$T_m = \sqrt{\frac{2m}{2N+1}}\,. \tag{2.43}$$

We now need to consider the integral

$$\int_{f_j}^{f_{T_n}} \frac{\mathrm{d}f}{\sqrt{2\mathcal{E} - 2V(f)}}\,, \tag{2.44}$$

in the $f \sim 1$ limit. In this case we take $f_j = 1 - \kappa$ to ensure the expansion is justified. We transform to the variable $h = 1 - f$ and find

$$\int_{\kappa T}^{\kappa} \frac{\mathrm{d}h}{\sqrt{2\mathcal{E} - 2V(h)}}\,, \tag{2.45}$$

where

$$V(h) = \kappa^2 \left(\frac{1}{2} - h\right) - \frac{1}{2}\left(4 - \kappa^2\right) h^2 + \mathcal{O}(h^3)\,. \tag{2.46}$$

By keeping only terms up to h^2 we account for all the κ dependence and the dominant effects of h in the $h \sim 0$ limit. This integral is evaluated to be

$$\frac{1}{2} \ln \frac{2\kappa + \sqrt{3\kappa^2 + 2\mathcal{E}}}{2\kappa T + \sqrt{(4T^2 - 1)\kappa^2 + 2\mathcal{E}}} + \mathcal{O}(\kappa)\,. \tag{2.47}$$

The other part of the integration is from f_- to f_j and is found to be

$$\int_{f_-}^{f_j} \mathrm{d}f \left[\frac{1}{f(1-f^2)} + \frac{f^2\kappa^2 - 2\mathcal{E}}{2f^3(1-f^2)^3} + \mathcal{O}(\kappa^4)\right] = \frac{1}{2} \ln \frac{1 - f_-^2}{2\kappa f_-^2} + \frac{1 - 2\mathcal{E}/\kappa^2}{32} + \mathcal{O}(\kappa)\,. \tag{2.48}$$

Then twice the total integral gives the estimate of $R^*_{N,\text{odd}} - R^*_{N,\text{even}}$:

$$\Delta_{\text{odd}} = \frac{1-2\mathcal{E}/\kappa^2}{16} + \ln\left[\frac{1-f_-^2}{2\kappa f_-^2}\frac{2\kappa+\sqrt{3\kappa^2+2\mathcal{E}}}{2\kappa T+\sqrt{(4T^2-1)\kappa^2+2\mathcal{E}}}\right]. \tag{2.49}$$

In summary, the radial distances $\Delta_n = R^*_{N,n} - R^*_{N,n-1}$ between radii are estimated to be

$$\Delta_n = \begin{cases} \ln\frac{2f_-^2}{\mathcal{E}_n(1-f_-^2)} & n \text{ even}, \\ \frac{1-2\mathcal{E}_n/\kappa^2}{16} + \ln\left[\frac{1-f_-^2}{2\kappa f_-^2}\frac{2\kappa+\sqrt{3\kappa^2+2\mathcal{E}_n}}{2\kappa T_{\frac{n-1}{2}}+\sqrt{(4T^2_{\frac{n-1}{2}}-1)\kappa^2+2\mathcal{E}_n}}\right] & n \text{ odd}, \end{cases} \tag{2.50}$$

$$= \begin{cases} -2\ln\kappa + \ln\left(\frac{2N+1}{N+1-n/2}\right) + \mathcal{O}(\kappa^2) & n \text{ even}, \\ -\ln\kappa + \frac{n-1}{16(2N+1)} + \frac{1}{2}\ln\left(\frac{(7-4\sqrt{3})(2N+1)\left(2+\sqrt{4+\frac{1-n}{2N+1}}\right)^2}{n-1}\right) + \mathcal{O}(\kappa^2) & n \text{ odd}, \end{cases} \tag{2.51}$$

with $2 \le n \le 2N+1$. Keeping only the leading log terms, we find the compact expression

$$R^*_{N,n} = R^*_{N,1} - \begin{cases} \left(\frac{3}{2}n-1\right)\ln\kappa + \mathcal{O}(\kappa^0), & \text{even } n, \\ \left(\frac{3}{2}n-\frac{3}{2}\right)\ln\kappa + \mathcal{O}(\kappa^0), & \text{odd } n, \end{cases} \tag{2.52}$$

for $1 \le n \le 2N+1$. We also know $R^*_{N,1} = (2N+1)/\kappa^2$ for small κ, but a better prediction requires the subleading terms that we derive in the following section.

2.3.3 Thick-Wall Limit

The description of an excited-state profile in terms of transition functions determined by $2N+1$ radii satisfying $f''(R^*_{N,n}) = 0$ is useful for small κ but breaks down at larger κ. Not

only the shape of f starts to differ, there also exists a threshold κ beyond which f'' only has $N+1$ zeros; all N radii with an even index in the above notation, $R^*_{N,2j}$, cease to satisfy $f''=0$, rendering our product of transition functions ansatz (2.24) unsuitable. Rather than changing our radius definition, we content ourselves with predicting the odd radii for $\kappa \sim 1$. Since this covers the first and last radius, it provides a useful idea of the soliton's extent.

Near $\kappa = 1$, in the thick-wall limit, we use a different approximation from above. In this case, we define $\varepsilon = 1-\kappa^2$ and consider $\varepsilon \ll 1$. The potential can then be written as

$$V(f) = -\frac{\varepsilon}{2}f^2 + f^4 - \frac{1}{2}f^6 \tag{2.53}$$

and therefore,

$$f'' + \frac{2}{\rho}f' - \varepsilon f + 4f^3 - 3f^5 = 0\,. \tag{2.54}$$

We then transform the equation into a rescaled profile and use a rescaled coordinate [62]:

$$f^2 = \varepsilon g^2, \qquad \rho^2 = z^2/\varepsilon\,. \tag{2.55}$$

The resulting equation is

$$g'' + \frac{2}{z}g' - g + 4g^3 - 3\varepsilon g^5 = 0\,, \tag{2.56}$$

N	$g(0)$	$c_{N,1}$	$c_{N,3}$	$c_{N,5}$	$c_{N,7}$	$c_{N,9}$
0	2.168693539	0.345758	–	–	–	–
1	7.051791599	0.106101	1.70188	–	–	–
2	14.565602713	0.0513571	0.793518	2.93172	–	–
3	24.6803496815	0.0303081	0.464925	1.64239	4.15909	–
4	37.38615404998	0.0200077	0.306252	1.0686	2.58726	5.39492

Table 2.1: Initial value $g(0)$ for use in shooting-method solutions to Eq. (2.56) with $\varepsilon = 0$ as well as coefficient values for Eq. (2.57).

and of course the boundary conditions of g are identical to f, that is $g'(0) = 0$ and $g(\infty) = 0$.

The leading order equation, with $\varepsilon \to 0$, can be solved generally for any N. A simple technique to use is the shooting method. By choosing $g(0)$ with $g'(0) = 0$ one can find approximate solutions to good accuracy. In Table 2.1, we record the initial values $g(0)$ as well as the radii—defined by $f'' = 0$—for several N. The radii diverge for $\kappa \to 1$ according to

$$R^*_{N,n} = \frac{c_{N,n}}{\sqrt{1-\kappa^2}}\,, \tag{2.57}$$

with coefficients $c_{N,n}$ given in Tab. 2.1. Note that the coefficient of the $1/\sqrt{1-\kappa^2}$ term for the $N = 0$ solitons matches very closely with the approximate fit found in Ref. [4].

Table 2.1 also shows that a given odd radius $R^*_{N,2j+1}$ *decreases* with N for fixed κ, unlike in the small κ limit where the radii *increase* linearly with N. The reason is that for $\kappa \sim 1$ and small N, the particle does not start anywhere near the maximum of the potential, so friction can not be neglected and complicates the intuition. However, at large enough N, the particles are unavoidably pushed towards the maximum and our arguments from before apply; at large N, the radii again grow with N, although that is not captured by Eq. (2.56) with $\varepsilon = 0$.

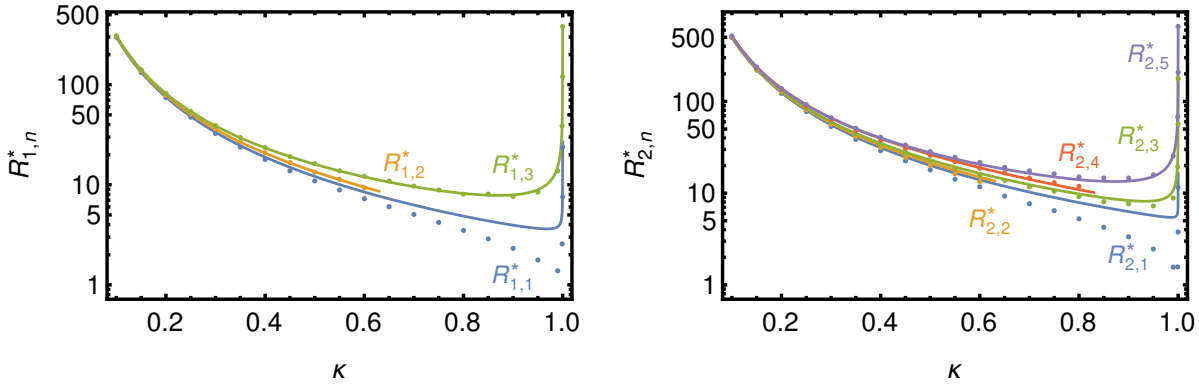

Figure 2.4: Left: the three radii $R^*_{1,n}$ vs. κ for the first excited state, $N = 1$. Dots are numerical results and the solid lines the prediction from Eq. (2.58). Right: radii for the $N = 2$ excited state together with the prediction from Eq. (2.58).

2.3.4 Final Predictions for the Radii

Having obtained approximations of the excited-state radii in the limiting cases of small and large κ we can combine them to obtain approximate radius predictions valid for all κ:

$$R^*_{N,n} = \frac{2N+1}{\kappa^2} + \begin{cases} \frac{c_{N,n-1}}{\sqrt{1-\kappa^2}} - \left(\frac{3}{2}n - 1\right)\ln\kappa\,, & \text{even } n\,, \\ \frac{c_{N,n}}{\sqrt{1-\kappa^2}} - \left(\frac{3}{2}n - \frac{3}{2}\right)\ln\kappa\,, & \text{odd } n\,. \end{cases} \tag{2.58}$$

where the coefficients $c_{N,n}$ can be read off from Tab. 2.1 and $n = 1, 2, 3, \ldots, 2N+1$. We mention again that the even radii, $R^*_{N,2k}$, no longer solve $f''(R^*_{N,2k}) = 0$ for large κ, so are no longer radii by our definition. All radii for the first and second excited states are shown in Fig. 2.4 and compared to numerical data. As expected, our predictions work well in the small and large κ regimes in which they were derived, but differ somewhat for κ in between.

The general behavior of $R^*_{N,n}$ vs. N is shown in Fig. 2.5. Notice that the naively expected behavior $R_{N+1,n} > R_{N,n}$ breaks down near $\kappa \sim 1$ because none of the particles are starting near the maximum f_+. For large enough N, this behavior would be restored though.

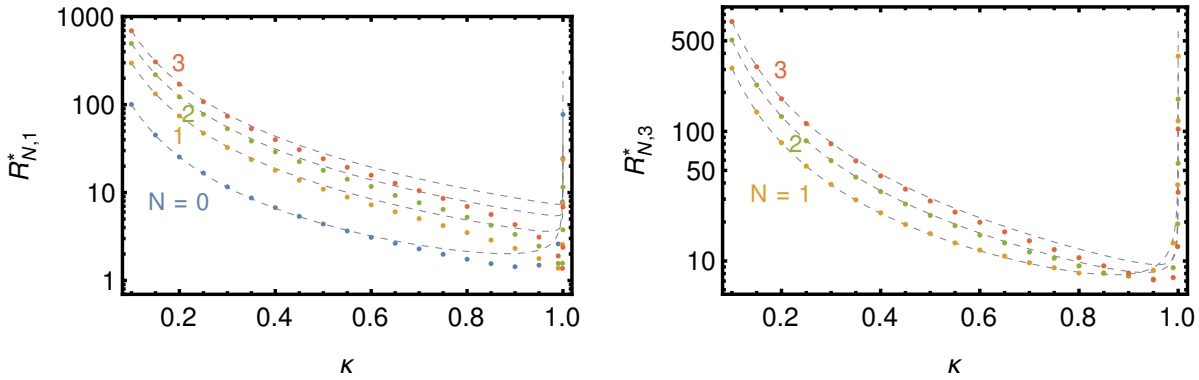

Figure 2.5: Transition radii $R^*_{N,1}$ (left) and $R^*_{N,3}$ (right) vs. κ for several N. Gray dashed lines are the approximations from Eq. (2.58).

2.4 Charge, Energy, and Stability

For small κ, we are able to predict the profile $f(\rho)$ for any excited state N to astonishing accuracy by combining the transition-profile ansatz from Eq. (2.24) with our radius predictions from Eq. (2.58). This then allows us to numerically calculate the integrals relevant for the Q-ball charge and energy, given in Eq. (2.10). Since analytical approximations quickly become bothersome, we restrict ourselves to the leading terms in small κ here.

Consider finding the value of the Q integral. As shown in Eq. (2.10), the nontrivial part takes the form $\int \mathrm{d}\rho\, \rho^2 f^2$ and in the $N = 0$ case [1], this takes the simple approximate value of $\int \mathrm{d}\rho\, \rho^2 f^2 = R_0^{*3}/3$ to leading order in R_0^*. If all the effects for an excited state N with $2N + 1$ transitions are included, we again find the leading-order result of

$$\int \mathrm{d}\rho\, \rho^2 f^2 = \frac{R_N^{*3}}{3}\,. \tag{2.59}$$

In this calculation we could have included a sum of N discrete $\Delta\,(R_N^*)^2$ contributions where Δ is the width of the excited state shell around the center soliton, but as $\Delta \ll R_N^*$, these contributions are subleading.

For the surface-energy integral $\int \mathrm{d}\rho\rho^2 f'^2$, the leading-order behavior is different. The $N = 0$ result [1] is $\int \mathrm{d}\rho\rho^2 f'^2 = R_0^{*2}/4$ to leading order in R_0^*. For excited states, the effects of additional transitions need to be summed over, using our knowledge from above that the differences between the radii, Δ, are large enough to separate the individual transitions, which yields

$$\int \mathrm{d}\rho\rho^2 f'^2 = (2N+1)\,\frac{R_N^{*2}}{4}\,. \tag{2.60}$$

It is significant that in this integral the f'^2 integral is proportional to the surface area at that radius, rather than a shell of volume.

Overall, using the leading order relation $R_N^* = (2N+1)/\kappa^2$, we find

$$\begin{aligned}\int \mathrm{d}\rho\,\rho^2 f^2 &\simeq \frac{(2N+1)^3}{3\kappa^6}\,,\\ \int \mathrm{d}\rho\,\rho^2 f'^2 &\simeq \frac{(2N+1)^3}{4\kappa^4}\,,\end{aligned} \tag{2.61}$$

for small κ, which can also be obtained by inserting our radius predictions (2.58) into the transition-profile ansatz (2.24) and evaluating the integrals. For $N = 0$, subleading terms have been derived in Ref. [1]. The comparison with numerical data in Fig. 2.6 shows that Eq. (2.61) is a fairly good approximation even for larger κ, and captures the N dependence very well. In fact, we find numerically that the scaling of the integrals with $(2N+1)^3$ is accurate far beyond the small-κ regime: simply rescaling the $N = 1$ integrals by $(2N+1)^3/(2+1)^3$ matches the $N = 2\ldots23$ integrals in the range $0 < \kappa \lesssim 0.9$ to better than 10% (20%) for $\int \mathrm{d}\rho\,\rho^2 f^2$ ($\int \mathrm{d}\rho\,\rho^2 f'^2$). This indicates that despite the excited Q-balls states having a more complicated structure compared to the ground state, the leading-order term $R_N^* = (2N+1)/\kappa^2$ is enough to characterize the properties of the excitation modes.

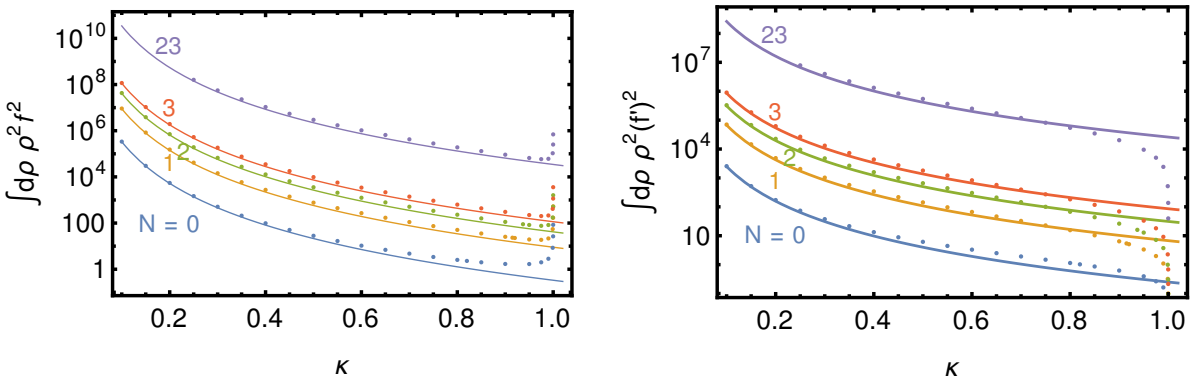

Figure 2.6: Integrals $\int \mathrm{d}\rho\, \rho^2 f^2$ (left) and $\int \mathrm{d}\rho\, \rho^2 f'^2$ (right) vs. κ—as relevant for Q-ball energy and charge—for the $N = 0$ ground state and several excited states. The solid lines show the small-κ approximations from Eq. (2.61).

The approximations in Eq. (2.61) as well as the general scaling with $(2N + 1)^3$ break down near $\kappa \sim 1$, but we can still understand the numerical behavior qualitatively. As shown above, in the thick-wall regime we expect the Q-ball radii to diverge according to $R_N^* \propto 1/\sqrt{1-\kappa^2}$. Since the integral $\int \mathrm{d}\rho\, \rho^2 f^2$ can be interpreted as the volume energy of the Q-ball [1], we also expect this integral to diverge for $\kappa \to 1$. The *surface* integral $\int \mathrm{d}\rho\, \rho^2 f'^2$, on the other hand, decreases because the Q-ball profile becomes increasingly dilute for $\kappa \to 1$, suppressing the derivatives [1].

Using the numerical integrals as a function of κ or the small-κ approximations, we obtain the Q-ball charge and energy via Eq. (2.10). The numerical results are illustrated in Fig. 2.7 for some example parameters. For small κ and $\omega_0 \neq 0$,[3] we find an expression for $E(Q)$ that is valid for large Q:

$$E(Q) \simeq \omega_0 Q + (2N+1) \left(\frac{\pi}{2}\right)^{1/3} \frac{3^{2/3}\sqrt{m_\phi^2 - \omega_0^2}}{2(\omega_0/\phi_0)^{2/3}} Q^{2/3} \tag{2.62}$$

and shows that excited states simply have a $2N + 1$ times larger surface energy than the ground state. Since the energy increases with N for fixed Q, we are correct in denoting these

[3]For $\omega_0 = 0$, the small-κ approximation is quite different and to leading order in large Q reads $E(Q) \simeq \frac{5}{2}\left(\frac{\pi}{3}\right)^{1/5}\left(N+\frac{1}{2}\right)^{3/5} m_\phi^{3/5}\phi_0^{2/5} Q^{4/5}$.

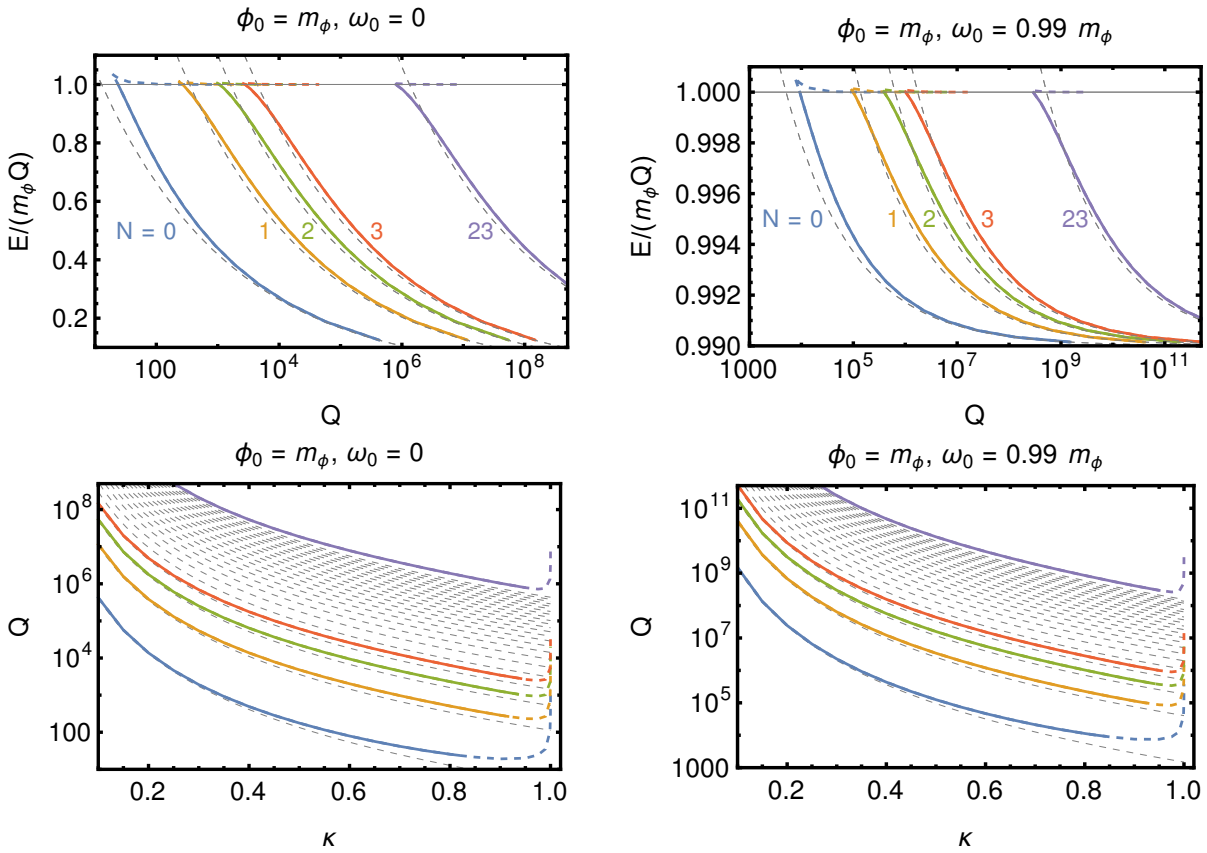

Figure 2.7: Top: $E/(m_\phi Q)$ vs. Q for $\omega_0 = 0$ (left) and $\omega_0 = 0.99 m_\phi$ (right) for the ground state ($N = 0$) and several excited states. In the regime with $E/(m_\phi Q) > 1$, the Q-ball can decay into Q free scalars, indicated by the dashed portion. The gray dashed lines denote our analytical large-Q predictions given in Eq. (2.62) and footnote 2. Bottom: Q vs. κ for the same examples. The gray dashed lines show the small-κ prediction $Q \propto (2N+1)^3/\kappa^6$ prediction from Eq. (2.61) for $N = 0$ to $N = 23$ to illustrate the density of states. Note that we arbitrarily stop at $N = 23$.

states as excited states, and assume they eventually decay into smaller Q-balls, as discussed below.[4]

In addition to energy, other components of the Q-ball energy–momentum tensor can also be approximated in the thin-wall limit. The scaling of several quantities with N for a fixed κ has been obtained in Ref. [32].

[4]The charge-swapped Q-ball states explored in Refs. [34, 35] may be quasi-stable.

2.4.1 Stability of Excited States

A detailed study of excited-state decays is postponed for future work, but let us nevertheless comment on stability. As shown in Ref. [1], the $N = 0$ states with $0 < \kappa \leq \kappa_{\text{stability}} \simeq 0.8$ are stable because they satisfy $E < m_\phi Q$ (and $\mathrm{d}Q/\mathrm{d}\omega < 0$ [64], which is a weaker stability criterion for our potential). The excited states with $N > 0$ are, on the other hand, unstable [59] and can decay into smaller Q-balls and/or individual scalars. From the above expression (2.62) it is clear that for sufficiently large N, the soliton will satisfy $E > m_\phi Q$, which then allows the Q-ball decay into Q individual ϕ scalars. This instability occurs at large κ, with a threshold that increases with N (see the dashed lines in Fig. 2.7). Even more energetically favorable than a decay into individual scalars is a decay into ground-state Q-balls, for which many possible final states are kinematically allowed. At large Q, excited states with $\kappa \sim 1$ have $E \simeq m_\phi Q$, while the ground state has $E \simeq \omega_0 Q$ (for $\omega_0 \neq 0$), so a configuration of k ground state Q-balls with charges that add up to Q still has a total energy around $\omega_0 Q$, which is smaller than $m_\phi Q$ by Eq. (2.3). Phase space arguments generically prefer a decay into few states.

The, arguably more interesting and slightly more stable, Q-balls with $E < m_\phi Q$ are well described by our small-κ expansion, at least for small N. These Q-balls cannot decay into Q scalars, but produce Q-balls with smaller Q in their final state; energetically, many final states are allowed [32]. From Fig. 2.7 it is easy to see that for a given N the condition $dQ/d\kappa < 0$ holds for most κ. In analogy with the ground state analysis, this implies that these solitons cannot decay to other states of the same N. However, they can decay into states with smaller N, except for the stable $N = 0$ case. By again using Eq. (2.62) as an approximation, we can also estimate the number of those excited states for a fixed Q as

$$N \simeq \frac{\sqrt{m_\phi^2 - \omega_0^2}}{3 m_\phi^{1/3} \phi_0^{2/3}} Q^{1/3}. \tag{2.63}$$

While there are infinitely many excited states for a fixed κ, the physically more relevant restriction to fixed Q only allows for a finite number of excitations. While angular excitations of Q-balls have been studied [31, 44], to our knowledge the number of excitations for fixed Q has not been specified. However, the known excited states satisfy $J = NQ$ for integers N which suggests there are only a finite number of angular excitations with energies below a given value, such as $E < m_\phi Q$.

Let us focus on the $N = 1$ excited state in the large-Q regime with $\omega_0 \neq 0$, so that we may use Eq. (2.62) as an approximation. One possible decay mode (and preferred by phase space considerations) is into two Q-balls of charge Q_1 and $Q - Q_1$, which have a lower energy of

$$E(Q_1)_{N=0} + E(Q-Q_1)_{N=0} - E(Q)_{N=1} \simeq -\left(\frac{\pi}{2}\right)^{1/3} \frac{3^{2/3}\sqrt{m_\phi^2 - \omega_0^2}}{2(\omega_0/\phi_0)^{2/3}} \times \left(3Q^{2/3} - (Q-Q_1)^{2/3} - Q_1^{2/3}\right). \quad (2.64)$$

The energy gain is minimized for $Q_1 = Q/2$, i.e. a decay into two ground-state Q-balls of equal charge, making this the least likely decay judging by phase space. More energy is released for $Q_1 \ll Q$, where our thin-wall expression from Eq. (2.62) breaks down for the smaller Q-ball. Let us consider the extreme case of the $N = 1$ decay into a $N = 0$ Q-ball of charge $Q - 1$ and a free scalar ϕ, with energy gap

$$E(Q-1)_{N=0} + E_\phi - E(Q)_{N=1} \simeq -2Q^{2/3}\left(\frac{\pi}{2}\right)^{1/3} \frac{3^{2/3}\sqrt{m_\phi^2 - \omega_0^2}}{2(\omega_0/\phi_0)^{2/3}}, \quad (2.65)$$

ignoring kinetic energies, so $E_\phi \simeq m_\phi$. For large Q, the ϕ mass is negligible so the same expression holds for the emission of additional scalars or scalar–anti-scalar pairs. Phase space will once again prefer a decay into few particles. Since the mass gap grows with $Q^{2/3}$, the lifetimes of large excited states are expected to be parametrically short, although the actual numbers depend on the values for the potential parameters.

2.5 Generalization To Other Potentials

So far our treatment of excited states has focused on the sextic potential of Eq. (2.11) as a definite example. In this section, we outline what aspects of our analysis are expected to be robust over many potentials that admit a thin-wall limit. We also highlight where differences between potentials play a significant role. These generalizations assume a single scalar field, leaving the analysis of multi-field models to future work.

We return, for the moment, to the basic requirements on the scalar potential for Q-ball solutions. It is useful to rewrite the conditions discussed in Sec. 2.2 on $U(|\phi|)$ in terms of the dimensionless potential

$$\widehat{U}(f) = \frac{1}{\phi_0^2(m_\phi^2 - \omega_0^2)} U(f\phi_0/\sqrt{2}) \ . \tag{2.66}$$

We find that

$$\widehat{U}(0) = 0 \ , \quad \left.\frac{\mathrm{d}\widehat{U}}{\mathrm{d}f}\right|_{f=0} = 0 \ , \quad \left.\frac{\mathrm{d}^2\widehat{U}}{\mathrm{d}f^2}\right|_{f=0} = \frac{m_\phi^2}{m_\phi^2 - \omega_0^2} \ . \tag{2.67}$$

The condition that $U(|\phi|)/|\phi|^2$ have a minimum at $\phi_0/\sqrt{2}$ is what allows for thin-wall solitons. This requirement is expressed as

$$\widehat{U}(1) = \frac{\omega_0^2}{2(m_\phi^2 - \omega_0^2)} \ , \quad \left.\frac{\mathrm{d}\widehat{U}}{\mathrm{d}f}\right|_{f=1} = \frac{\omega_0^2}{m_\phi^2 - \omega_0^2} \ , \quad \left.\frac{\mathrm{d}^2\widehat{U}}{\mathrm{d}f^2}\right|_{f=1} > \frac{\omega_0^2}{m_\phi^2 - \omega_0^2} \ . \tag{2.68}$$

We can then determine the extrema of $V(f)$, the effective potential that appears in the

equations of motion. The locations of the extrema are determined by

$$\frac{\mathrm{d}\widehat{U}}{\mathrm{d}f} = f\frac{\omega^2}{m_\phi^2 - \omega_0^2} \ . \tag{2.69}$$

The second derivative of $V(f)$ reveals maxima and minima:

$$\frac{\mathrm{d}^2 V}{\mathrm{d}f^2} = \frac{\omega^2}{m_\phi^2 - \omega_0^2} - \frac{\mathrm{d}^2\widehat{U}}{\mathrm{d}f^2} \ . \tag{2.70}$$

For instance, we have an extremum at $f = 0$ with

$$\left.\frac{\mathrm{d}^2 V}{\mathrm{d}f^2}\right|_{f=0} = \frac{\omega^2 - m_\phi^2}{m_\phi^2 - \omega_0^2} \leq 0 \ . \tag{2.71}$$

This is less than zero because $\omega \leq m_\phi$, so this is a maximum except at $\omega = m_\phi$. We also see that $V(f)$ has an extremum at $f = 1$, but only when $\omega = \omega_0$, the thin-wall limit. In this case

$$\left.\frac{\mathrm{d}^2 V}{\mathrm{d}f^2}\right|_{f=1} = \frac{\omega_0^2 - m_\phi^2}{m_\phi^2 - \omega_0^2} = -1 \ , \tag{2.72}$$

so this is also a maximum. Clearly, there must be at least one minimum between these two maxima. However, depending of the specifics of $U(|\phi|)$ there may be other extrema as well. The salient point is that any potential that satisfies the requirements to support thin-wall Q-balls has a local maximum at $f = 1$ when $\omega = \omega_0$.

By construction, $V(0) = 0$. We also have $V(1) = 0$ when $\omega = \omega_0$. This means that in the $\omega = \omega_0$ limit, the "particle" may transition from the $f = 1$ maximum and end at the $f = 0$ maximum only after waiting an infinite amount of "time" (related to infinite radius for the Q-ball) before transitioning. When it does transition it rolls without friction, meaning there is a conserved energy

$$\mathcal{E} = \frac{1}{2} f'^2 + V(f) \ . \tag{2.73}$$

This can be extracted directly from the equations of motion (2.8) in the infinite ρ limit

$$\frac{\mathrm{d}}{\mathrm{d}\rho}\left(\frac{1}{2} f'^2 + V(f)\right) = 0 \ . \tag{2.74}$$

In this "thin-wall" limit the particle is at rest at $\rho = 0$ ($f = 0$) and at $\rho = \infty$ ($f = 1$). Therefore, both of these points have $\mathcal{E} = 0$. This special trajectory, what we have called the transition function f_T, satisfies

$$\frac{\mathrm{d}f_T}{\mathrm{d}\rho} = -\sqrt{-2V(f_T)} \ . \tag{2.75}$$

The negative root must be chosen to ensure f_T decreases with increasing ρ.

For the sextic potential this equation leads to Eq. (2.14), but it is well defined for any potential that gives rise to Q-balls. Albeit generally impossible to solve analytically, Eq. (2.75) is trivial to integrate numerically, providing an approximate thin-wall solution to the original differential equation. As shown above, these transition functions are the building blocks from which radial Q-ball modes are constructed. In this chapter our numerical results show

this explicitly with the sextic potential. However, our final approximate analytical result for the N-th excited state profile (2.24) is given in terms of f_T to indicate how our the results that follow from this profile are expected to generalize to other potentials.

In the thin-wall limit, $\omega \to \omega_0$, the profile form given in (2.24) must be correct. In this case, the particle rolls without friction and makes N transitions without friction between the maxima at $f = \pm 1$ and $f = 0$. Each of these transitions is given by the function defined above. We have seen that for the sextic potential they remain a good approximation well away from this limit, but for more complicated potentials this agreement may break down sooner.

Despite being derived for our particular sextic potential, we expect the $E(Q)$ result of Eq. (2.62) to be approximately valid for all potentials that exhibit a thin-wall limit, since it relies mainly on the N scaling of the integrals in Eqs. (2.59) and (2.60). For large Q and small N, radially excited states simply increase the Q-ball energy by $2N$ times the surface energy. The spectrum is surprisingly simple and can be estimated using ground-state properties (volume and surface energies).

2.6 Conclusion

Q-balls are simple non-topological solitons that can be interpreted as bound states of $U(1)$-symmetric scalars. The ground state solutions in a wide range of parameter space are stable because they furnish the smallest-energy configuration for a fixed $U(1)$ charge Q. As with other bound-state systems, excited Q-balls states with energies above the ground state can exist as well.

These excited states can play an essential role in accurately describing soliton production as well as the dynamics of soliton scattering. From the standpoint of these physical motivations

the excited state spectrum for fixed charge Q is most important. We have provided the first characterization of this spectrum, focusing on the sextic potential. In particular, we have shown that Q-balls of fixed Q have a finite number of radial excitations. This number grows with Q and some smaller solitons have only a few excited states of this type or even none at all.

We have developed a qualitative understanding of the radial excitations of Q-ball solitons and provided accurate approximate solutions. Our results are sufficient to describe the properties of arbitrary excited states in the sextic potential and should carry over with minimal modifications to other cases. While we have commented on the (in)stability of these excited states the difficult task of calculating the decay rates into smaller ground-state Q-balls and/or individual scalars is left for future work.

Chapter 3

Excited Gauged Q-balls

This chapter is heavily based on a paper [].

3.1 Introduction

By promoting the $U(1)$ to a local symmetry, gauged Q-balls arise [66] where we have a scalar and gauged fields coupled to one another. Gauged Q-balls have properties that are distinct from global Q-balls such as having a maximal possible size, and charge [67, 68]. Studying these properties analytically by solving the two sets of coupled nonlinear equations in the gauged Q-ball set-up does not seem like a feasible strategy with the level of complexity each equation brings to the table. Luckily, a mapping relation between gauged and global Q-ball ground state was discovered in Ref. [4], which reduces the gauged Q-ball problem into essentially a global Q-ball one. Despite the differences between gauged and global Q-balls due to having the extra gauged field, the scalar field of the gauged Q-ball is still expected to admit radial excitations. Interestingly, radial excitations of gauged Q-balls in sextic potential have been studied in Ref. [69] where it was shown that excited states of gauged Q-balls also

posses some unique properties compared to excited global Q-balls. For example, it was shown that the number of allowable excitations is finite for gauged Q-balls, whereas, it is infinite for global Q-balls.

In this chapter, we build on the success of the mapping relation in characterizing unexcited gauged Q-balls in terms of unexcited global Q-balls by extending the map to excited gauged Q-balls. By doing so, we find analytical expressions describing properties of these states such as the maximum possible number of excitation gauged Q-balls could acquire, and the maximum size of these Q-balls. We also demonstrate approximations of the charge and energy in the large radius limit deduced from the mapping relation for the unexcited gauged Q-balls discovered in Ref. [4] holds for excited gauged Q-ball and we comment on their instabilities. This implies that despite excited gauged Q-balls richer structure their properties are characterized by the leading order term of the radii similar to the ground state. In our charge and energy discussion, we point out that in certain regions of the gauged Q-ball parameter space the energy gap between excited states and the ground state is small, which suggest a longer lifetime for the excited states. Moreover, the numerical success of extending the mapping relation is also illustrated by using the finite element method to produce exact profiles of excited gauged Q-balls.

This chapter is organized as follows. We start the discussion in Sec. 3.2 by first reviewing unexcited and excited global Q-balls, unexcited gauged Q-balls, and how unexcited gauged and global Q-balls are related to one another via the mapping. In Sec. 3.4, we show how extending the mapping relation provide an easy tool to obtain numerical profiles of excited gauged Q-balls. Analytical limits are derived for the maximum number of excitations a gauged Q-ball could have and the maximum possible radius for each excitation in Sec. 3.5 via the mapping relation. Comparisons between the numerical and analytical prediction are shown in the same section. In Sec. 3.6, we demonstrate the success of the charge and energy approximations in estimating the exact values of these quantities in the excited gauged Q-

ball case in the large radius limit. We also point out that for certain regions of the parameter space excited gauged Q-balls could have longer lifetime due to the small energy gap with the ground stand and discuss different instability regions. The conclusion is presented in Sec. 3.7.

3.2 Excited Q-balls Radii Leading Order

We re-emphasize one of the key findings of the previous chapter in this section as it will play a key role in the mapping excited gauged Q-balls. In the thin wall limit (κ_G is small), the ground state of global Q-ball radius that is defined as $f''(R_0^*) = 0$, is approximated by [1]

$$R_0^*(\kappa) = \frac{1}{\kappa_G^2}\,. \tag{3.1}$$

For the Nth excited state of a global Q-ball we expect $(2N+1)$ radii $R_{N,n}^*$ satisfying $f''(R_{N,n}^*) = 0$ where n is an integer that goes from 1 to N as shown in Eq. (2.58). However, the leading order term of the radii

$$R_N^*(\kappa) = \frac{(2N+1)}{\kappa_G^2}\,, \tag{3.2}$$

is enough to approximate the properties of the excited states. The position of this quantity is not well defined in terms of the profile but the Q-ball properties and the conventional radii $R_{N,n}^*$ are derived from this length scale as shown in previous chapter. Observable such as the charge Q_G and energy E_G of global Q-balls are expressed in terms of the following integrals

$$Q_G = \frac{4\pi\phi_0^2\omega_G}{(m_\phi^2-\omega_0^2)^{3/2}}\int \mathrm{d}\rho\,\rho^2 f^2\,, \tag{3.3}$$

$$E_G = \omega Q_G + \frac{4\pi\phi_0^2}{3\sqrt{m_\phi^2 - \omega_0^2}} \int \mathrm{d}\rho\, \rho^2 f'^2\,, \tag{3.4}$$

satisfying the the Q-ball condition $dE_G/d\omega = \omega dQ_G/d\omega$ [59, 63, 1]. The integrals are approximated to be

$$\int \mathrm{d}\rho\, \rho^2 f^2 \simeq \frac{(2N+1)^3}{3\kappa_G^6}\,, \tag{3.5}$$

$$\int \mathrm{d}\rho\, \rho^2 f'^2 \simeq \frac{(2N+1)^3}{4\kappa_G^4}\,, \tag{3.6}$$

as shown in Ch. 2 allowing us to estimate the observables in terms of κ_G for all excited states of a given Q-ball in the thin wall (large radius) limit. Therefore, in this chapter when discussing the radius of excited Q-balls we will refer to this leading order term even though it does not satisfy the radius definition of the ground state. In terms of notation in this chapter, the subscript G will be reserved to global Q-balls parameters and properties $\{\kappa_G, Q_G, E_G\}$ to distinguish them from their gauged counterpart.

3.3 Gauged Q-balls

Promoting the $U(1)$ to a local symmetry gives rise to gauged Q-balls. The Lagrange density for gauged Q-balls is

$$\mathcal{L} = |D_\mu \phi|^2 - U(|\phi|) - \frac{1}{4} F_{\mu\nu} F^{\mu\nu}, \tag{3.7}$$

where $D_\mu = \partial_\mu - ieA_\mu$ is the covariant derivative, $F_{\mu\nu} = \partial_\mu A_\nu - \partial_\nu A_\mu$ is the field-strength tensor, and e is the normalized gauge coupling to insure ϕ has charge one. The scalar and gauged field can be written following the static charge ansatz from Ref. [66] as

$$\phi(t,\vec{x}) = \frac{\phi_0}{\sqrt{2}} f(r) e^{i\omega t}, \quad A_0(t,\vec{x}) \equiv A_0(r), \quad A_i(t,\vec{x}) = 0\,. \tag{3.8}$$

The scalar frequency of gauged Q-balls is bounded by $\omega_0 < \omega \leq m_\phi$, which differs slightly from the global case where $\omega \neq m_\phi$ [67]. Re-defining our parameters in terms of dimensionless quantities

$$A(\rho) \equiv \frac{A_0(\rho)}{\phi_0}, \quad \Omega \equiv \frac{\omega}{\sqrt{m_\phi^2 - \omega_0^2}}\,, \quad \alpha \equiv e\Phi_0\,, \quad \kappa \equiv \Omega^2 - \Omega_0^2\,, \quad \Phi_0 \equiv \frac{\phi_0}{\sqrt{m_\phi^2 - \omega_0^2}}\,, \tag{3.9}$$

giving us the following Lagrangian

$$\mathcal{L} = 4\pi\Phi_0^2\sqrt{m_\phi^2 - \omega_0^2}\int d\rho\rho^2 \left[-\frac{1}{2}f'^2 + \frac{1}{2}A'^2 + \frac{1}{2}f^2(\Omega^2 - \alpha A)^2 - \frac{U(f)}{\Phi_0^2(m_\phi^2 - \omega_0^2)^2}\right], \tag{3.10}$$

with the effective potential being

$$V(f,A) = \frac{1}{2}f^2\left(\Omega - \alpha A\right)^2 - \frac{U(f)}{\Phi_0^2(m_\phi^2 - \omega_0^2)^2} = \frac{1}{2}f^2\left[\kappa^2 + \alpha A(\alpha A - 2\Omega) - \left(1 - f^2\right)^2\right], \tag{3.11}$$

where we have expressed $V(f,A)$ in terms of the sextic potential. The effective potential in the the gauged Q-ball case depends on two fields f and A producing two equations of motions

$$f'' + \frac{2}{\rho}f' = -\frac{\partial V}{\partial f} = \frac{1}{\Phi_0^2(m_\phi^2 - \omega_0^2)^2}\frac{\mathrm{d}U}{\mathrm{d}f} - \left(\Omega - \alpha A\right)^2 f\,, \tag{3.12}$$

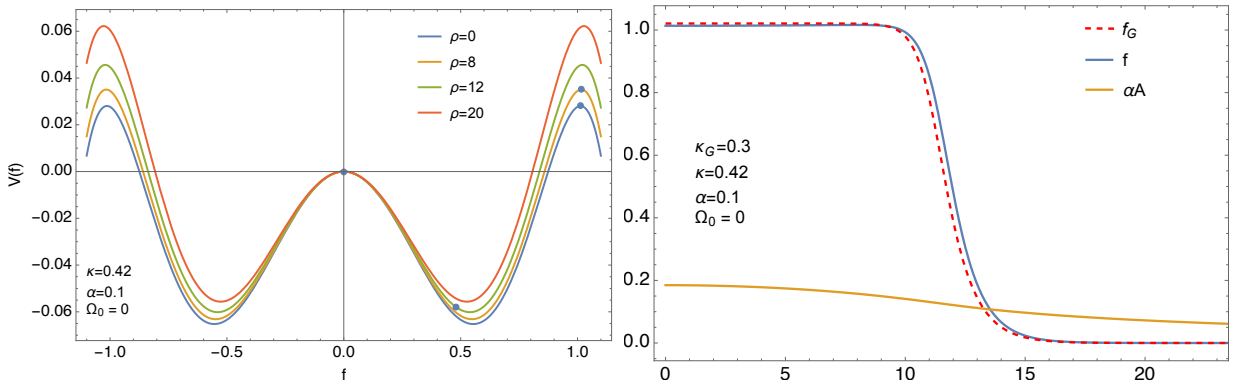

Figure 3.1: Effective potential of the gauged Q-ball changing with $A(\rho)$ vs f and the black dots representing the value of the scalar field for each ρ (left). Exact profiles of the gauged Q-ball denoted by the solid lines and the global Q-ball that maps to the specified gauged Q-ball denoted by the dashed line (right).

$$A'' + \frac{2}{\rho}A' = +\frac{\partial V}{\partial A} = \alpha f^2(A\alpha - \Omega)\,, \tag{3.13}$$

with the boundary condition being

$$\lim_{\rho\to 0} f' = \lim_{\rho\to\infty} f = \lim_{\rho\to 0} A' = \lim_{\rho\to\infty} A = 0\,. \tag{3.14}$$

Notice that in that the kinetic term of A carries the opposite sign. This introduces a subtle distinction between the scalar field f and the gauge field A analysis in terms of the effective potential. Contrary to the scalar field, the gauge field A is expected to start at somewhere downhill on the effective potential and get pushed upward toward the $A(\rho \to \infty) = 0$. The effective potential has a minimum in terms of the gauge field when f is constant at

$$A_{\max} = \frac{\Omega}{\alpha}\,, \tag{3.15}$$

and depending on the initial value of A, the gauged field would either go to zero or infinity for $\rho \to \infty$. Therefore, we expect that the initial $\Omega - \alpha A > 0$ to satisfy the boundary condition for gauged Q-balls to exist, otherwise the gauge field will go to infinity [4].

On the other hand the scalar field f equation of motion in the gauged set-up, similar to the

global case, is analogous to a particle rolling in the potential with time-dependent friction with the caveat that the $V(f, A)$ is dynamical in ρ since A changes with the radius (Fig. 3.1). The particle still can roll N time past $f = 0$ before ending up there satisfying the boundary condition, which gives rise to excited gauged Q-ball solutions. The effective potential has three extrema when A is constant one is at $f = 0$ and the other two are at

$$f_{\pm}^2 = \frac{1}{3}\left(2 \pm \sqrt{1 + 3\kappa^2 - 3\alpha A(2\Omega - \alpha A)}\right), \tag{3.16}$$

where f_+ is the maximum and f_- is the minimum. The extrema introduces a boundary condition on αA as shown in [4]

$$\alpha A \leq \Omega - \sqrt{\Omega_0^2 - 1/3}\,, \tag{3.17}$$

when $\Omega_0 \leq 1/\sqrt{3}$. The other boundary $\alpha A \geq \Omega - \sqrt{\Omega_0^2 - 1/3}$ is excluded since it violates the gauged Q-ball condition $\Omega - \alpha A > 0$ as illustrated earlier. Observables of gauged Q-balls such as charge and energy [66, 4] are expressed as

$$Q = \frac{4\pi\phi_0^2}{(m_\phi^2 - \omega_0^2)} \int \mathrm{d}\rho\, \rho^2 f^2 \left(\Omega - \alpha A\right), \tag{3.18}$$

$$E = \omega Q + \frac{4\pi\phi_0^2}{3\sqrt{m_\phi^2 - \omega_0^2}} \int \mathrm{d}\rho\, \rho^2 \left(f'^2 - A'^2\right), \tag{3.19}$$

satisfying $dE/d\omega = \omega dQ/d\omega$ [65] .

Numerically solving the gauged Q-ball problem via the shooting method is doable but rather tedious and describing the properties of these solution is even harder with two field dependent

on one another. Therefore, as shown in [4], a successful method in reducing the gauged Q-ball problem is by realizing there is a mapping equation between gauged and global Q-balls, which simplifies the analysis numerically and analytically. The map is derived by first solving the equation of motion of A Eq.(3.13) in the thin-wall limit where the scalar field can be approximated in terms of a step-function $f(\rho) = 1 - \Theta(\rho - R^*)$ [66]

$$A(\rho) = \frac{\Omega}{\alpha} \begin{cases} 1 - \dfrac{\sinh(\alpha\rho)}{\cosh(\alpha R^*)\,\alpha\rho}\,, & \rho < R^*\,, \\ \dfrac{\alpha R^* - \tanh(\alpha R^*)}{\alpha\rho}\,, & \rho \geq R^*\,. \end{cases} \tag{3.20}$$

In this limit, when the radius of the Q-ball is large, the change in αA is expected to be small since $\alpha A' < \Omega/R^*$ meaning the scalar field equation of motion at $\rho \sim R^*$ can be written as

$$f'' + \frac{2}{\rho} f' = \frac{1}{\Phi_0^2(m_\phi^2 - \omega_0^2)^2} \frac{\mathrm{d}U}{\mathrm{d}f} - \left[\Omega - \alpha A(R^*)\right]^2 f\,, \tag{3.21}$$

which is identical to the global Q-ball equation of motion (Eq.(**??**)) if we identify

$$\Omega_G = \Omega - \alpha A(R^*)\,. \tag{3.22}$$

By substituting Eq.(3.20) in Eq.(3.22) we get the mapping relation

$$\Omega(R^*) = \Omega_G(R^*)\,\alpha R^* \coth(\alpha R^*)\,. \tag{3.23}$$

This relation was derived in Ref. [4], and the numerical and analytical success of the mapping equation, even beyond the thin-wall limit, in describing the gauged Q-ball ground was

demonstrated in that article. Regardless of the value of κ, the finite element method with the mapping relation could numerically produce the ground state of gauged Q-balls profiles (Fig. 3.1). Also, analytical approximations of the maximum radius, charge, and energy of gauged Q-ball ground state, that match the numerical finding, has been derived in the thin-wall limit via the mapping relation. In the next sections, we extend the mapping relation to excited states of gauged Q-balls in order to expand the numerical and analytical analysis to cover the full gauged Q-ball space.

3.4 Excited Gauged Q-balls Profiles

To numerically compute excited gauged Q-ball profiles using the finite element method [4, 70, 71] in *Mathematica*, we re-write our equations of motion in terms of our compactified coordinate y

$$\left(1-\frac{y}{a}\right)^4\left(f''+\frac{2}{y}f'\right)+f\left(\kappa^2+\alpha A(\alpha A-2\Omega)-1+4f^2-3f^4\right)=0\,, \tag{3.24}$$

$$\left(1-\frac{y}{a}\right)^4\left(A''+\frac{2}{y}A'\right)-\alpha f^2\left(\alpha A-\Omega\right)=0\,, \tag{3.25}$$

where $y=\frac{\rho}{1+\frac{\rho}{a}}$ and a is a positive number, which is assumed to be large compared to the Q-ball radius. Therefore, the boundary conditions in terms of our new coordinate are

$$f(a)=f'(0)=A(a)=A'(0)=0\,. \tag{3.26}$$

The difference between the the ground state and the excited state is in the initial seed function for the scalar field f, and the radius R_N^* relationship to κ_G as shown in Eq.(3.2). The mapping equation (Eq.(3.23)) is successful in computing κ for all possible excited states of gauged Q-balls with coupling α, and Ω_0 parameter. Even though excited (global/gauged)

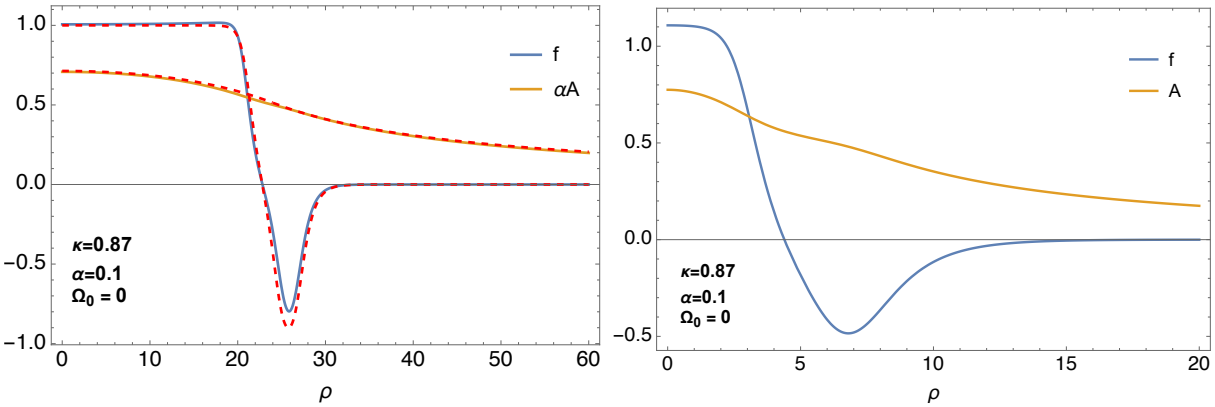

Figure 3.2: Exact profile of first excited state of gauged Q-ball in the thin-wall limit denoted by the solid line, and the thin-wall approximations from Eq.(2.24) and Eq.(3.20) are denoted by the dashed line (left). Exact profiles of first excited state of gauged Q-ball beyond the thin-wall limit denoted by the solid line (right).

Q-balls have $(2N+1)$ radii satisfying $f''(R_{N,n}) = 0$ as pointed in the review section, R_N^* is enough to determine the properties of these configurations. Numerically, this is illustrated by Fig. 3.2 where excited gauged Q-ball profiles are obtained by only specifying R_N^* in the finite element method code and this is generally true for all excited states. In Fig. 3.2 we also show that Eq.(2.24) and Eq.(3.20) provide good approximations of the scalar f and gauge A, in the thin-wall limit, and the approximations break beyond that limit. To use Eq.(2.24) as shown in Fig. 3.2, one needs to provide $R_{N,n}$, which can either be extracted from the numerical profile at $f''(R_{N,n}) = 0$ or analytically predicted using Eq.(2.58). Numerical solutions do not exist for arbitrary large N excitations of gauged Q-balls, as illustrated in Ref. [69], and in the next section we will use the mapping relation to approximate an analytical upper bound on the maximum number of possible excited states per gauged Q-ball.

3.5 Approximations of Excited Gauged Q-balls Properties

The mapping relation cannot be solved analytically, however, approximations have been deduced for unexcited gauged Q-balls by understanding the limiting cases of the mapping

function [4]. And as we showed in the previous section, the mapping equation can be extended to predict excited states, therefore, we try to find generalized analytical approximations of our gauged Q-ball space. Recall that in the thin-limit, the radius (leading order term) of excited Q-balls is approximated by $R_N^* = (2N+1)/\kappa_G^2$ (Eq.(3.2)), thus, the map can be re-written in terms of κ_G

$$\kappa^2 = \frac{\tilde{\alpha}^2}{\kappa_G^2}(1+\frac{\Omega_0^2}{\kappa_G^2})\coth^2(\frac{\tilde{\alpha}}{\kappa_G^2}) - \Omega_0^2\,, \tag{3.27}$$

where $\tilde{\alpha} = (2N+1)\alpha$. Notice that the equation is now identical to the ground state mapping relation. This allows us to use the analytical expression that was derived in [4]

$$\tilde{\alpha} \lesssim \frac{1}{\sqrt{1/0.58^2 + 9\Omega_0^2/2}}\,, \tag{3.28}$$

in order to further understand the excited gauged Q-ball properties. By re-writing the the bound in terms of α and N

$$N_{\max} \lesssim \frac{1}{2\alpha\sqrt{1/0.58^2 + 9\Omega_0^2/2}} - \frac{1}{2}\,, \tag{3.29}$$

we obtain an upper limit on the number of the excited states a gauged Q-ball could acquire. This bound agrees with the findings from Ref. [69] where it was shown that excited gauged Q-balls have a finite number of excited states, which is inversely proportional to the coupling implying that a minimum coupling value ($\alpha \approx 0.182$) is required for an excited state to exist. Now, we have an analytical expression which can quantitatively approximate the maximum number of excited states a gauged Q-ball can acquire depending on the gauged coupling α and the parameter Ω_0.

The mapping equation clearly implies that κ is larger for higher excited states of gauged Q-balls with a certain radius since $\tilde{\alpha}$ increases with N. Also, the nature of coth function Eq.(3.27) coupled with the bound $\kappa \leq 1$ entail a decrease in the radii space for higher

excitation. By imposing the upper bound ($\kappa = 1$), we get the following equation

$$1 = \frac{\tilde{\alpha}^2}{\kappa_G^2}\left(1 + \frac{\Omega_0^2}{\kappa_G^2}\right)\coth^2\left(\frac{\tilde{\alpha}}{\kappa_G^2}\right) - \Omega_0^2\,, \tag{3.30}$$

which allows us to analytically approximate the maximum $R^*_{N(\max)}$ (thin-wall limit) in terms of α, Ω_0 and N. As mentioned earlier the mapping equation is not analytically solvable but we can deduce $R^*_{N(\max)}$ limits for regions when $\alpha \gtrsim \Omega_0$ and $\tilde{\alpha} << \Omega_0$. In the first case, the maximum radius is approximated to be

$$R^*_{N(\max)} \simeq \frac{1}{(2N+1)\,\alpha^2}\,, \qquad \alpha \gtrsim \Omega_0\,, \tag{3.31}$$

for all N excited states with α gauged coupling. This analytical approximation works because when substituting in the mapping equation it reduces to

$$\left(1 + \frac{\Omega_0^2}{(2N+1)\alpha^2}\right)\coth^2\left(\frac{1}{(2N+1)\alpha}\right) - \Omega_0^2 = 1\,, \tag{3.32}$$

where the second and third term are small compared to the first term and the second term gets smaller for larger N. The approximation works for arbitrary α and N since the number of excited states are inversely proportional to the gauge coupling as demonstrated by Eq.(3.29). This relation implies that $\coth^2(1/((2N+1)\alpha)) \approx 1$ for all N as there will not be enough excited states per gauged coupling that will increase the value of the function significantly. For the second case when $\tilde{\alpha} << \Omega_0$ ground state limit for the maximum

$$R^*_{N(\max)} \simeq \frac{1}{\alpha\Omega_0}\,, \qquad \tilde{\alpha} << \Omega_0\,, \tag{3.33}$$

holds. In the second case, unlike the first one, the approximation does not work for arbitrary N but is restricted by $(2N+1)\alpha << \Omega_0$ and this can be seen by substituting the radius

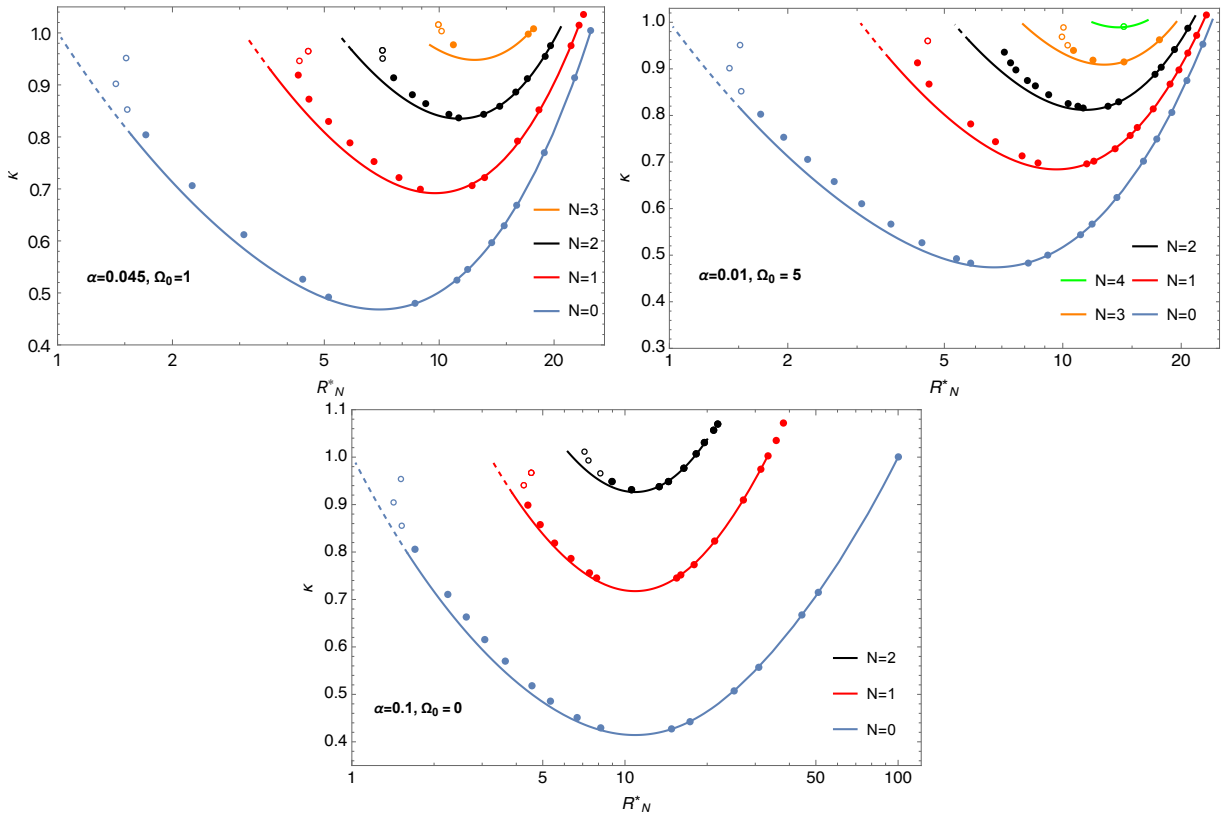

Figure 3.3: Exact values of κ vs R_N^* for all possible excited states of gauged Q-balls denoted by the dots compared to the analytical prediction from the mapping equation and the radii approximation from Eq.(3.27) and Eq.(3.2). Different benchmarks are shown: $\alpha = 0.045$, $\Omega_0 = 1$ (top left), $\alpha = 0.01$, $\Omega_0 = 5$ (top right), and $\alpha = 0.1$, $\Omega_0 = 0$ (bottom). Solid lines and dots denotes the Q-ball region where $E \leq m_\phi Q$ is satisfied.

again in the mapping equation (Eq.(3.23))

$$\left(\frac{\alpha(2N+1)}{\Omega_0}+1\right)\coth^2\left(\frac{1}{\Omega_0}\right)-\Omega_0^2=1\,, \tag{3.34}$$

The second term is independent of N and clearly larger than the first term for the specified region allowing for the approximation of the maximum radius to hold.

We chose three different combinations of α and Ω_0 in Fig. 3.3 to demonstrate the approximated limits we found for maximum number of excited states a gauged Q-ball could acquire and the maximum radius admitted per state. For each state analytical κ vs R_N^* has been plotted using Eq.(3.2) for the radii and the mapping relation Eq.(3.25) for κ. Smaller radii are expected to have higher order corrections that are harder to obtain, however, the thin-

wall approximation is sufficient for our discussion. Exact numerical radii of excited gauged Q-balls are represented by the dots in the figure and they match very well with the analytical solution. Finding distinct exact solutions becomes harder in the region where the variation in the value of κ is very small (Fig. 3.3).

The upper limit on $N_{\max}$ is illustrated numerically and analytically for different α and Ω_0 benchmarks in Fig. 3.3. For $\alpha = 0.01$ and $\Omega_0 = 5$ benchmark, the maximum possible excited state would be at $N_{\max} = 4$ as shown analytically and numerically, which agrees with Eq.(3.29) where $N_{\max} \lesssim 4.15$. Also, Fig. 3.3 demonstrates our finding from Eq.(3.31) and Eq.(3.33). In the the example where $\Omega_0 = 0$ the maximum radius decreases with larger excited states and matches our approximation from Eq.(3.31). However, when $\Omega_0 \gg \tilde{\alpha}$ it is apparent that the maximum radii cluster around the limit we show in Eq.(3.33). As mentioned earlier, the second approximation does not hold for all N, and this is apparent in $N = 3$ excited state when $\Omega_0 = 1$.

It is evident from our discussion that the space of possible solutions per excited gauged Q-ball shrinks for higher states. We can infer qualitatively from the mapping equation and $\kappa \leq 1$ that the minimum radius increases for higher excited states, even though finding an analytical expression for the minimum radius is complicated beyond the thin-wall limit. The smaller the region of possible radii and the κ, the harder it is to find distinct numerical solutions, which explains the small number of exact solutions provided for higher excited states in Fig. 3.3. We re-iterate that the radius approximation we use does not capture the exact behaviour for smaller radii since we expect higher order terms to become relevant in this region for excited states adjusting the shape of the radii curves just like the ground states shown in Ref. [4]. This is going to be beyond the scope of this thesis, but could be an interesting topic to investigate to improve the findings beyond the thin wall limit. In the plots you would notice that the curves and dots are divided into solid and dashed segments representing different instability regions, which we will discuss in the next section.

3.6 Charge, Energy and Stability

Excited gauged Q-balls are unstable configurations, and to determine the type of instability and where a occurs, we must discuss the charge and energy of of these states. The charge Q and energy E of gauged Q-balls as shown in Sec.3.2 are given by

$$Q = \frac{4\pi\phi_0^2}{m_\phi^2 - \omega_0^2} \int d\rho \rho^2 f^2 (\Omega - \alpha A), \tag{3.35}$$

$$E = \omega Q + \frac{4\pi\phi_0^2}{3\sqrt{m_\phi^2 - \omega_0^2}} \int d\rho \rho^2 (f'^2 - A'^2). \tag{3.36}$$

The exact integrals are numerically calculable over the profiles we produced in Sec. 3.4 and shown as dots in Fig. 3.4. Since the mapping relation worked for excited states, the approximation of charge and energy derived in [4] of the ground state of gauged Q-ball in the large radius limit could be extended to estimate the observables for the excited states

$$Q_N = \frac{4\pi\Omega\Phi_0^2}{\alpha^3} \left(\alpha R_N^* - \tanh\left(\alpha R_N^*\right)\right) \tag{3.37}$$

$$E_N = \omega Q_N + \frac{\pi\phi_0^2 R_N^{*2}}{3\sqrt{m_\phi^2 - \omega_0^2}} - \frac{\pi\phi_0^2}{3\sqrt{m_\phi^2 - \omega_0^2}} \frac{\Omega^2(\alpha R_N^*(\mathrm{sech}(\alpha R_N^*) + 2) - 3\tanh(\alpha R_N^*))}{2\alpha^3}, \tag{3.38}$$

as shown in Fig. 3.4. This demonstrates the point we made in Sec. 3.4 where we argued that properties of excited gauged Q-balls are determined by the value of R_N^* despite the states having $(2N+1)$ radii satisfying $f''(R_{n,N}) = 0$.

As we have seen in the previous section, κ of gauged Q-balls increase for higher excited

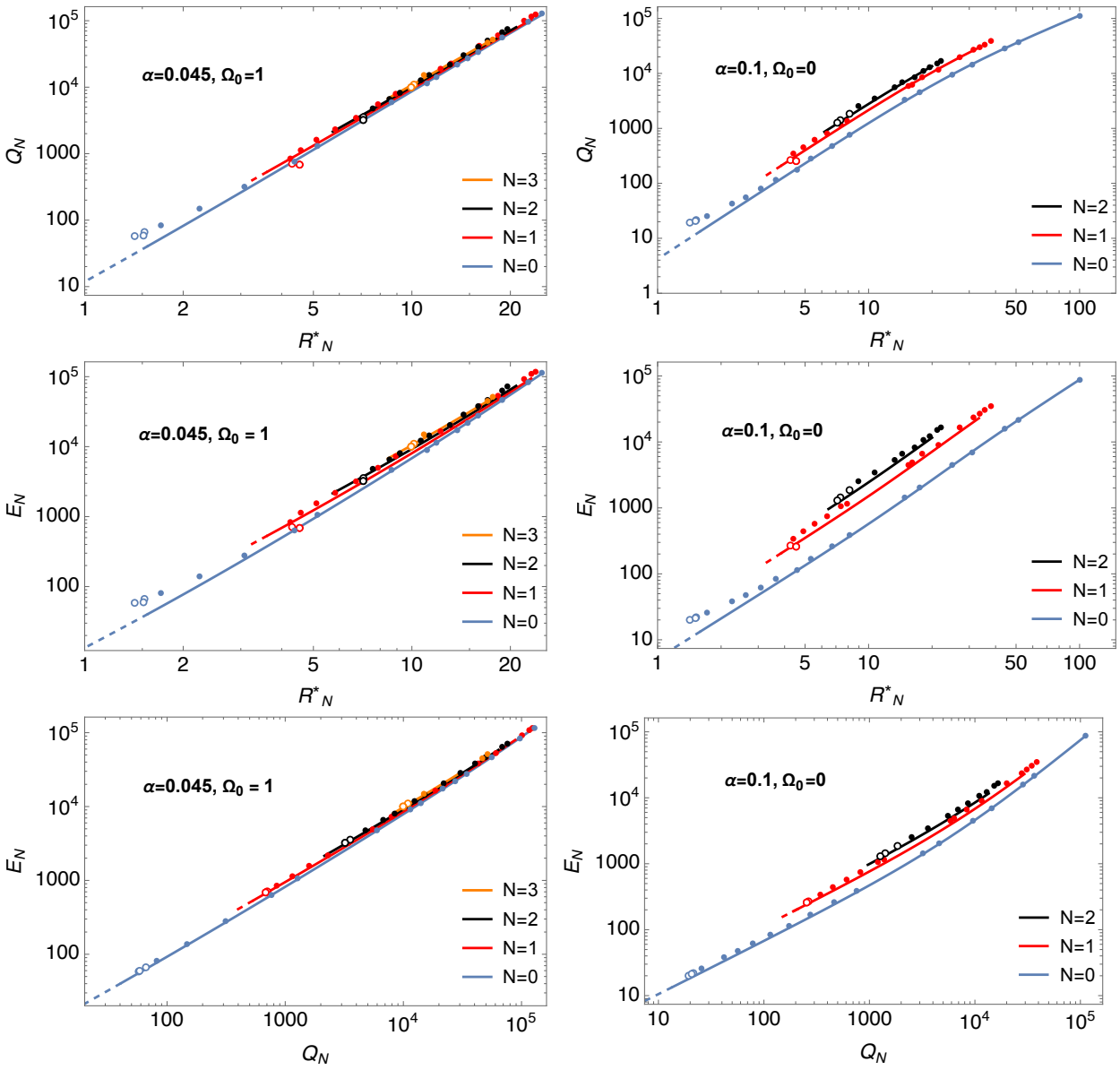

Figure 3.4: Exact values of charge and energy vs R^*_N and energy vs charge for all possible states of gauged Q-balls denoted by the dots compared to the analytical thin-wall predictions from Eq.(3.37-3.38). Different benchmarks are shown: $\alpha = 0.045$, $\Omega_0 = 1$ (left), and $\alpha = 0.1$, $\Omega_0 = 0$ (right). Solid lines and dots denotes the Q-ball region where $E \leq m_\phi Q$ is satisfied and $m_\phi = \phi_0 = 1$ for all benchmarks.

states of the same radius, which implies that the charge and energy increase for higher excited states. Curiously though, larger Ω_0 will dominate the expressions $\Omega^2 = \kappa^2 + \Omega_0^2$ decreasing the influence of changing κ for higher excited states. This is shown in Fig.3.4, where we see that the charge and energy for the example with $\Omega_0 = 0$ increase for higher excited states. However, when increasing $\Omega_0 = 1$, the distinction between the charge and energy of each state diminishes. This implies that excited states of gauged Q-balls with larger Ω_0 would have have a longer lifetime since the energy gap ΔE gets smaller with the ground state and the lifetime is inversely proportional to the energy gap. This is illustrated by the E vs Q plot in Fig.3.4 this is because when comparing energies of different level of excitations of the *same* gauged Q-ball, we should describe the gauged Q-ball with the *same* charge. It is important to emphasize that these approximations are better for larger R_N^* or smaller κ, however, they deviate from the exact values beyond the limit.

Another way of discussing the charge and energy of excited Q-balls would be in terms of the number of excitations, which is going to be useful to discuss stability. If we think of our charge and energies integrals in terms of κ_G, a natural relation emerges between the states. The gauged Q-ball charge Q (Eq.(3.35) can essentially be written in terms of the global Q-ball charge Q_G since the map Eq.(3.22) tells us that $\Omega_G = \Omega - \alpha A$. The difference between the charge of the gauged Q-ball and the global Q-ball is that in the gauged case the charge has an upper bound due to the existence of a maximum radius as demonstrated in the previous section. The integral approximation of $\rho^2 f^2$ shown in Eq.(3.5) implies that the charge of excited gauged Q-balls are expressed as

$$Q_N(\kappa_G) = (2N+1)^3 Q_0(\kappa_G) \propto \frac{(2N+1)^3}{3\kappa^6}\,, \tag{3.39}$$

where $Q_0(\kappa_G)$ is the charge of the ground state. Similarly, the energy of excited gauged Q-balls can be written in terms of the ground state energy $E_0(\kappa_G)$ by using the integral

approximation of $\rho^2 f'^2$ from Eq.(3.6)

$$E_N(\kappa_G) = (2N+1)^3 E_0(\kappa_G) \propto \frac{(2N+1)^3}{4\kappa_G^4}\,, \tag{3.40}$$

This approximation evidently ignores the contribution from A' integral from Eq.(3.38) and is valid only when $\kappa_G \gtrsim 0.2$, otherwise the the approximation breaks down as the the contribution becomes significant. This approximation could still be relevant for excited gauged Q-balls despite the lower bound on κ_G since the maximum radius is expected to get smaller for higher excite states, as shown in Eq.(3.31) and Eq.(3.33) meaning the minimum κ_G gets pushed to a larger value. This results captures the significance of the mapping relation where properties that are harder to estimate in the gauged Q-ball set-up could be expressed in terms of global Q-ball properties (Fig. 3.5).

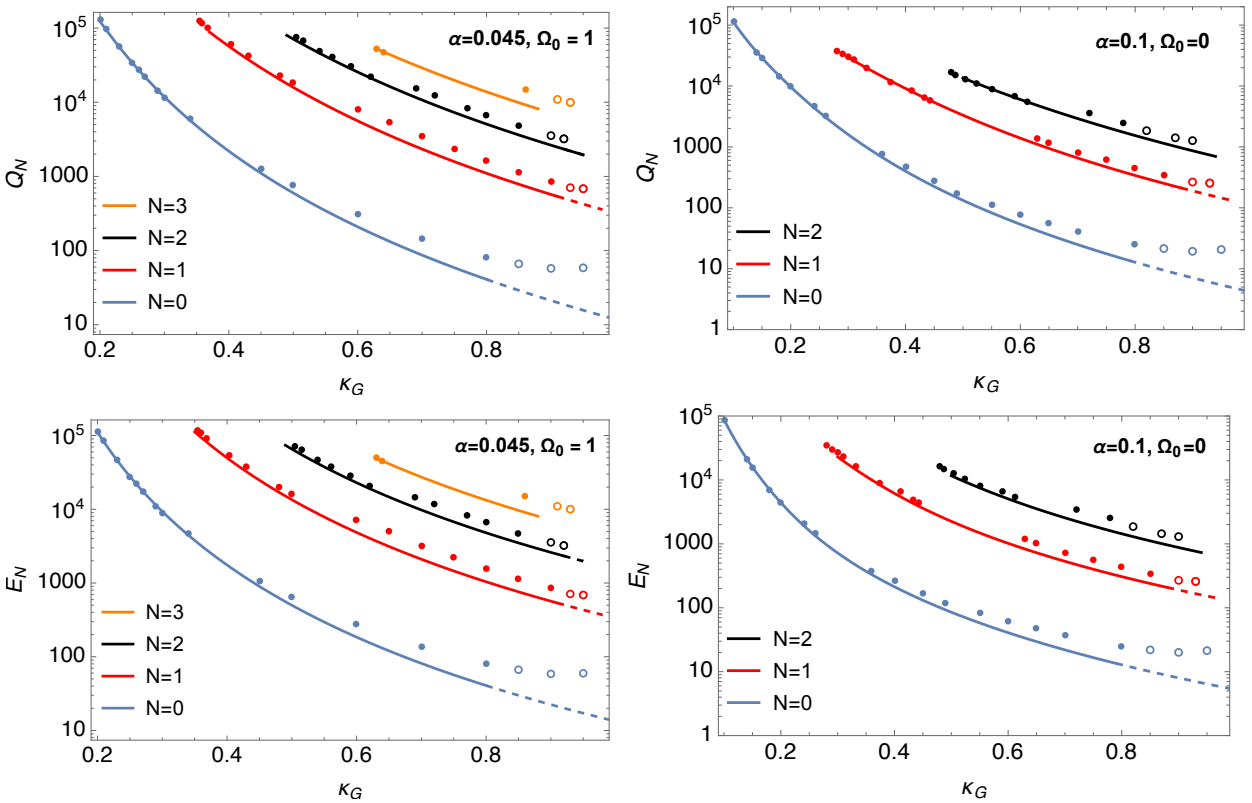

Figure 3.5: Exact values of charge and energy vs κ_G for all possible excited states of gauged Q-balls denoted by the dots compared to the analytical thin-wall predictions from Eq.(3.39-3.40). Different benchmarks are shown: $\alpha = 0.045$, $\Omega_0 = 1$ (left), and $\alpha = 0.1$, $\Omega_0 = 0$ (right). Solid lines and dots denotes the Q-ball region where $E \leq m_\phi Q$ is satisfied and $m_\phi = \phi_0 = 1$ for all benchmarks.

Excited (global and gauged) Q-balls are unstable configurations [59, 4, 69]. The first instability comes from the the condition that requires $E \leq m_\phi Q$ for Q-balls to be stable against decay completely into free scalars. The condition is satisfied for the gauged and global Q-ball ground state when $\kappa_G \lesssim 0.84$, which implies that the minimal stable radius is expected around $R^* \simeq 1.5$. Therefore, for excited gauged Q-balls we would expect the minimal radius satisfying $E \leq m_\phi Q$ condition to approximately be around $R^* \simeq (2N+1)/\kappa^2_{G,stability}$ if the radius relation to κ holds where $\kappa_{G,stability}$ increases for excited states. However, as we pointed out earlier, in this region higher order corrections become relevant meaning this approximation is not reliable and we should rely on the numerical results. This explains the disagreement in the minimum stable radius between analytical approximation curves and the exact solutions shown in Fig. 3.6, where the exact minimum radius is larger than our approximation.

Even though the Q-ball configuration is stable when $E \leq m_\phi Q$, excited gauged Q-balls are not stable in this region against decay into Q-balls with lower energy by emitting scalars. This fact can be illustrated by writing the energy of the excited gauged Q-balls in term of their charge. Since approximations in Eq.(3.39-3.40) hold in the thin-wall limit, the gauged Q-ball case, similar to the excited global Q-ball case, we could re-write the energy in terms of the charge when $\kappa_G \gtrsim 0.2$

$$E(Q)_{\omega_0=0} \simeq \frac{5}{2}(\frac{\pi m_\phi^3 \phi_0^2}{3})^{1/5}(2N+1)^{3/5}Q^{4/5}\,, \tag{3.41}$$

$$E(Q)_{\omega_0\neq 0} \simeq \omega_0 Q + (2N+1)(\frac{\pi}{3})^{1/3}\frac{3^{2/3}\sqrt{m_\phi^2-\omega_0^2}}{2(\omega_0/\phi_0)^{2/3}}Q^{2/3}\,. \tag{3.42}$$

This expression can be used to demonstrate that it is energetically more favorable for an excited Q-balls to decay into a ground state Q-ball by emitting scalars instead of breaking

into a number of smaller Q-balls as shown in Chapter 2 for global excited Q-balls.

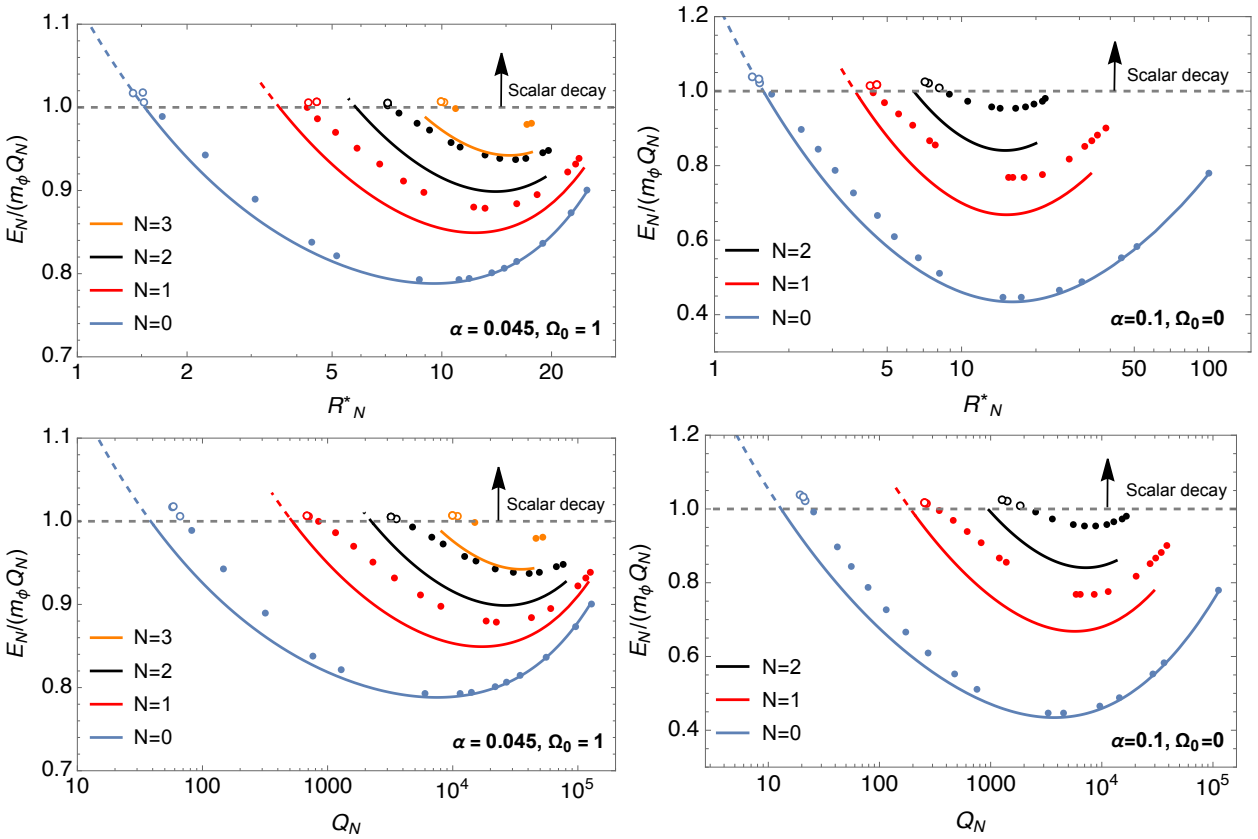

Figure 3.6: Exact values of $E/(m_\phi Q)$ vs R_N^* (top) and Q (bottom) for all possible excited states of gauged Q-balls denoted by the dots compared to the analytical thin-wall approximations from Eq.(3.37-3.38). Excited gauged Q-balls with $E/(m_\phi Q) > 1$ decay into Q free scalar, while $E/(m_\phi Q) \leq 1$ decay into ground state Q-balls by emitting free scalars. Different benchmarks are shown: $\alpha = 0.045$, $\Omega_0 = 1$ (left), and $\alpha = 0.1$, $\Omega_0 = 0$ (right). $m_\phi = \phi_0 = 1$ for all benchmarks.

3.7 Conclusion

The success of describing unexcited gauged Q-balls properties via the mapping relation in terms of the simpler global Q-ball has inspired this article where we extend the method to discuss excited gauged Q-balls. The extension allows us to numerically obtain solutions for all the excited states and analytically derive expressions that approximates the properties of these states in the thin wall limit. It was shown that regardless of the excitation level, properties of gauged Q-balls are described by a the leading order term of the radii similae

to the unexcited gauged Q-balls.

This is demonstrated in the chapter by numerically producing excited gauged Q-ball profiles via the finite element method allowing us to compute exact properties such as radius, charge and energy of each excited state. Using the mapping relation, we derived an analytical expression that approximates the upper bound on the number of excited states a gauged Q-balls can posses. In the thin wall limit, analytical limits on the maximal radius are estimated in certain regions of the parameter space and approximate expressions of the charge and energy are produced for all excited states in terms of the excitation level. We discuss the possibility of having excited gauged Q-balls with larger lifetimes in certain parameter space where the energy gap between the excited states and ground state are shown to be smaller. We also show that analytical results are in good agreement with the exact results produced numerically in the large radius limit and close by discussing the unstable nature of these excited gauged Q-balls.

In conclusion, the mapping relation proved to be successful in describing gauged Q-balls in terms of global Q-balls beyond the ground state. The map produced an analytical approximation limit on the number of excited states a gauged Q-ball can acquire. Excited gauged Q-balls can be produced numerically using the finite element method, and analytical approximation are reliable in predicting the properties of these states in the thin-wall limit by specifying a single radius. Some regions of the parameter space admit excited gauged Q-ball with longer lifetime, which might be worth further investigation for potential phenomenological implications if the lifetime is large enough by properly studying the decay rates. Finding higher order corrections to small radii could also improve the analytical approximations.

Chapter 4

Slowly Rotating Q-balls

This chapter is heavily based on work previously published in collaboration with Julian Heeck, Arvind Rajaraman, and Christopher B. Verhaaren [].

4.1 Introduction

In the Q-balls discussions, it is usually assumed that miniclusters with angular momentum can still collapse into Q-balls. This is a normal assumption for collapse to black holes or disks, for which any angular momentum is allowed. However, for rotating Q-balls [31, 38, 39, 40, 41, 42] (and the closely related boson stars [43, 44, 45, 46, 47, 48, 49, 50, 51, 52, 53, 54, 55]) the dominant paradigm is that the angular momentum must be an integer multiple of the charge Q. If this is the case, then the formation of large Q-balls would be drastically different from the usual collapse, since angular momentum would need to be shed in a very precise manner.

This is, in fact, a puzzling scenario since one might expect that a large classical object like a Q-ball could be given a small angular velocity by adding, for instance, a single particle

with nonzero angular momentum about the center of the soliton. This would naively give the final object a small angular momentum. Classically, at least, these are continuous quantities, and one expects to be able to make the angular velocity and angular momentum arbitrarily small. Naturally, the angular momentum is quantized in the quantum theory, but even so, one would expect that it should be possible to place a small number of particles in a state of nonzero angular momentum, so that the angular momentum of the Q-ball does not scale with the total charge and the reported quantization of Q-ball angular momentum is a purely classical effect.

In this chapter, we revisit these issues. We begin with a brief history of rotating boson stars, which were analyzed some years before rotating Q-balls. The first published analysis of boson star rotation [72] performed a perturbative analysis which indicated that boson stars cannot slowly rotate. However, the authors of this analysis only considered axisymmetric perturbations of the gravitational metric and the scalar field, with no dependence on the azimuthal angle φ. While axisymmetric perturbations are sufficient to support angular momentum in the gravitational portions of such a system, an axisymmetric scalar field configuration carries no angular momentum. (For a quick review of this fact see Appendix A.1.) Consequently, the axisymmetric ansatz is ill suited for fully exploring the rotation of boson stars. While it may give insight into angular momentum carried by the gravitational field the axisymmetric assumption precludes the scalar field from carrying any angular momentum.

Indeed, subsequent numerical studies which produced rotating boson stars assume a φ dependent scalar field with a profile of the form

$$f(r, \theta, \varphi) = g(r, \theta) \exp(iN\varphi)\,, \tag{4.1}$$

for some integer N. Beginning with [73, 74], these investigation found that the angular

momentum J of the boson star satisfies $J = NQ$, where Q is the particle number of the star.[1] However, as noted in these first analyses, this quantization of the boson star angular momentum follows directly from the form of the scalar profile assumed in Eq. (4.1). While the numerical construction of solutions that fit this profile is clearly significant, the fact that those solutions exhibit quantized angular momenta can only be seen as a consequence of the assumed form of the scalar field.

Therefore, the question remains, if a more general ansatz is employed, one that does not begin with the *assumption* $J = NQ$, can rotating boson stars be found with a different relationship between the angular momentum and particle number? In order to disentangle gravitational effects and focus on the dynamics of the scalar field, in this chapter we confine ourselves to the simpler case of rotating Q-balls. So far, all rotating Q-ball solutions have also assumed a scalar field configuration like Eq. (4.1). Consequently, the solutions have all exhibited $J = NQ$, with the implications for Q-ball production discussed above.

In this chapter we analyze the classical equations of motion and consider a more general perturbation around the nonrotating Q-ball than previous analyses. This perturbation allows for small rotations. We find that to leading order in the small angular velocity μ, there is indeed a perturbation which has nonzero angular momentum and is localized near the Q-ball; specifically the profile of the perturbation falls off exponentially far away from the Q-ball. For scalar potentials that produce nonlinearities in the equations of motion, however, higher orders in the perturbation expansion cannot be self-consistently taken to vanish.[2] The generic expectation is that for both Q-balls and boson stars we must include higher order terms, some of which are likely to be oscillatory and fall off only as fast as $1/r$. These contributions suggest that our perturbative ansatz that allows for small rotation also leads to the radiation of energy and angular momentum and is hence an unstable field configuration, not a true

[1] Similar proportionalities of charge and angular momentum have been found in other soliton systems, see e.g. Refs. [75, 76].

[2] Some boson stars with simple potentials for the scalar field may not require these higher order modes, however, the nonlinear gravitational interactions require a dedicated study.

solution to the field equations.

The effect of this instability is characterized in order to provide an estimate of the life-time of the localized, rotating perturbation. This is done by calculating the radiated power due to the oscillating modes and comparing that to the energy of the localized, rotating perturbation. For all Q-balls potentials, we find that the decay life-time of this perturbation due to radiation can be very long if the perturbation is small enough. As a consequence, the process of collapsing miniclusters can proceed as usual, at least for sufficiently slow rotation.

After reviewing nonrotating Q-balls in the following section, and setting up our notation, we motivate and present our new more general ansatz for rotating Q-balls in Sec. 4.2. The ansatz is based on the expansion of the scalar field in terms of spherical harmonics Y_{LM}, with the Y_{00} term taken to be a nonrotating Q-ball. This allows us to smoothly go to the nonrotating Q-ball limit by taking the $L \neq 0$ modes to zero. Similarly, we can consider small perturbations away from the known nonrotating solutions by taking these modes to be proportional to $\varepsilon \ll 1$.

These higher L modes also involve a new parameter μ, which we show to correspond to the angular velocity of the Q-ball in Appendix A.1. For $\varepsilon \ll 1$ and small angular velocities (Sec. 4.3), we find an analytical solution to the equations of motion of the Q-balls to leading order in ε and μ for all scalar potentials that lead to Q-balls. Aspects of higher order corrections to this solution are discussed in Sec. 4.4 with several details provided in Appendix A.2. These sections outline at what order radiating modes might be sourced by the initial perturbation. We also estimate the lifetime of the metastable rotating state by evaluating the equivalent of the Poynting vector for this scalar field configuration. At the classical level, we find that slowly rotating, radiating states can persist for cosmological times. We close with a discussion of our results in Sec. 4.5

4.2 Rotating Q-balls

Before delving into the rotating Q-balls discussion, we will re-write the non-rotating Q-ball ansatz as

$$\phi(t,\vec{x}) = \Phi_0(r=|\vec{x}|)e^{-i\omega t} \equiv \frac{\phi_0}{\sqrt{2}} f(r) e^{-i\omega t}\,. \tag{4.2}$$

Therefore, we could express the Q-ball equation of motion as

$$-\omega^2\Phi_0 - \nabla^2\Phi_0 + \frac{\partial U(|\Phi_0|^2)}{\partial \Phi_0^*} = 0. \tag{4.3}$$

A dimensionless potential is written as

$$\overline{U}(|\Phi|^2) = \frac{U(|\Phi|^2)}{\phi_0^2(m_\phi^2 - \omega_0^2)}\ . \tag{4.4}$$

It is more useful in this chapter to discuss the equations of motion of Q-balls in terms of the potential in this chapter instead of the effective potential, and this will become apparent when we explore the slowly rotating Q-ball anstaz.

Now, let us turn our attention to the rotating case. Clearly, rotating Q-balls cannot be spherically symmetric, or else the angular momentum $\vec{J}$ would be zero. For a scalar field this is also true of axisymmetric configurations, as shown in Appendix A.1. In particular, the z component of $\vec{J}$ is given by

$$J_z = -\int \mathrm{d}^3x \left(\dot{\Phi}\partial_\varphi\Phi^* + \dot{\Phi}^*\partial_\varphi\Phi\right) \tag{4.5}$$

in spherical coordinates. For a nonzero J_z, the field Φ must therefore depend on the azimuthal angle φ.

Typically [31, 38, 39, 40, 42, 43, 44, 45, 46, 47, 48, 49, 50, 51, 54], the profile for the scalar field of a rotating Q-ball or boson star is assumed to take the form

$$\Phi(t, r, \theta, \varphi) = f(r, \theta) e^{iN\varphi} e^{-i\omega t} \tag{4.6}$$

with integer N, which leads to $J_x = J_y = 0$ and

$$J_z = iN \int \mathrm{d}^3x \left(\Phi^* \dot{\Phi} - \dot{\Phi}^* \Phi \right) = NQ \,. \tag{4.7}$$

Note that this follows completely from the form of Eq. (4.6), without any reference to equations of motion. Consequently, any scalar field configuration, soliton or not, of the form given in Eq. (4.6) satisfies $J = NQ$. If this field configuration has a large Q, then making this ansatz amounts to assuming that the field cannot have small angular momentum. Numerical solutions for $f(r, \theta)$ have been found, providing evidence for the existence of rotating Q-balls whose angular momentum scales with the charge.

However, it is not obvious that the φ dependence in the scalar field must take the simple form of (4.6). To explore the possibility of Q-balls with $|J_z| \ll Q$, we must consider a more general ansatz where the profile contains different components with different φ dependence:

$$\Phi = \frac{\phi_0}{\sqrt{2}} \left[f(r) e^{-i\omega t} + \sum_{L,M} h_{LM}(r, t) Y_{LM}(\theta, \varphi) \right], \tag{4.8}$$

where the Y_{LM} are the usual spherical harmonics; an $L = 0$ term can be absorbed into $f(r)$

so the sum begins with $L = 1$. As these ansatzes are continuously connected to the non-rotating solution $\Phi_0 e^{-i\omega t}$, one expects that perturbations of this form, including those with angular momentum, can be made arbitrarily small, unlike in the ansatz (4.6). For example if the h_{LM} are small, this could correspond to the introduction of a few particles, possibly including some with angular momentum relative to the center of the soliton, to a nonrotating Q-ball.

To motivate a suitable ansatz for the time dependence, we note that the ground states of rotating Q-balls should have the lowest energy with a fixed charge Q and angular momentum J_z. These are found by introducing two Lagrange multipliers ω and μ, and minimizing the functional

$$E_{\omega,\mu} = E + \omega \left[Q - i \int \mathrm{d}^3x (\Phi^* \dot{\Phi} - \Phi \dot{\Phi}^*) \right] + \mu \left[J_z + \int \mathrm{d}^3x \left(\dot{\Phi}^* \partial_\varphi \Phi + \dot{\Phi} \partial_\varphi \Phi^* \right) \right] \tag{4.9}$$

$$= \omega Q + \mu J_z + \int \mathrm{d}^3x \left[|\dot{\Phi} + i\omega\Phi + \mu \partial_\varphi \Phi|^2 + |\nabla \Phi|^2 + U - |i\omega\Phi + \mu \partial_\varphi \Phi|^2 \right] . \tag{4.10}$$

Minimizing the first term in the integral leads to

$$\dot{\Phi} + i\omega\Phi + \mu \partial_\varphi \Phi = 0 \,, \tag{4.11}$$

which ensures that charge, angular momentum about the z-axis, and energy are time independent. Eq. (4.11) also implies that

$$h_{LM}(r,t) = h_{LM}(r) e^{-i(\omega + M\mu)t} \,. \tag{4.12}$$

Applying Eq. (4.11) allows us to write the energy (2.9) as

$$E = \omega Q + \mu J_z - \mathcal{L} \ , \tag{4.13}$$

where the Lagrangian $\mathcal{L}$ is given by

$$\mathcal{L} = \int \mathrm{d}^3x \left[\omega^2|\Phi|^2 + \mu^2 \left|\partial_\varphi \Phi\right|^2 + i\omega\mu \left(\Phi\partial_\varphi\Phi^* - \Phi^*\partial_\varphi\Phi\right) - |\nabla\Phi|^2 - U\right] \ . \tag{4.14}$$

For fields that satisfy the equations of motion, one can show that

$$\frac{\mathrm{d}\mathcal{L}}{\mathrm{d}\omega} = Q \ , \quad \frac{\mathrm{d}\mathcal{L}}{\mathrm{d}\mu} = J_z \ . \tag{4.15}$$

Straightforward calculations produce the relations

$$\begin{aligned} \frac{\mathrm{d}E}{\mathrm{d}\omega} &= Q + \omega\frac{\mathrm{d}Q}{\mathrm{d}\omega} + \mu\frac{\mathrm{d}J_z}{\mathrm{d}\omega} - \frac{\mathrm{d}\mathcal{L}}{\mathrm{d}\omega} \\ &= \omega\frac{\mathrm{d}Q}{\mathrm{d}\omega} + \mu\frac{\mathrm{d}J_z}{\mathrm{d}\omega} \, , \end{aligned} \tag{4.16}$$

$$\begin{aligned} \frac{\mathrm{d}E}{\mathrm{d}\mu} &= \omega\frac{\mathrm{d}Q}{\mathrm{d}\mu} + J_z + \mu\frac{\mathrm{d}J_z}{\mathrm{d}\mu} - \frac{\mathrm{d}\mathcal{L}}{\mathrm{d}\mu} \\ &= \omega\frac{\mathrm{d}Q}{\mathrm{d}\mu} + \mu\frac{\mathrm{d}J_z}{\mathrm{d}\mu} \, . \end{aligned} \tag{4.17}$$

In other words, we see that $dE/d\omega = \omega dQ/d\omega$ is generalized to

$$\mathrm{d}E = \omega \, \mathrm{d}Q + \mu \, \mathrm{d}J_z \, . \tag{4.18}$$

Since μ is conjugate to J_z, it should be related to the angular velocity of the soliton about the z-axis. This is also seen in the form of our ansatz (4.12), which depends on the combination $\varphi - \mu t$. Finally, it is shown in the appendix A.1 that

$$\frac{\mathrm{d}J_x}{\mathrm{d}t} = -\mu J_y \,, \qquad \frac{\mathrm{d}J_y}{\mathrm{d}t} = \mu J_x \,, \tag{4.19}$$

which correspond to the Euler equations of a rotating rigid body in the absence of external torques, when μ is taken to be the angular velocity about the z-axis.

Notice that the well-known ansatz from Eq. (4.6) is rather special: since J_z and Q are not independent in this ansatz, μ and ω are not independent either and always show up as a fixed linear combination $\omega + N\mu$. Existing numerical solutions do not reference μ, even though they find solitons with nonzero angular velocity. These works effectively absorb μ into their working definition of ω. Our above formalism is useful precisely for the opposite scenario in which J_z and Q can be varied independently.

4.3 A Small J_z Solution

As we construct the equations that determine the ansatz (4.8), in the limit of small J_z, we use the spherical harmonic convention $Y^*_{L,M} = (-1)^M Y_{L,-M}$. This allows us to write

$$\Phi^* = \frac{\phi_0}{\sqrt{2}} \left[f e^{i\omega t} + \sum_{L,M} h^*_{L,-M} (-1)^M Y_{LM} e^{i(\omega - M\mu)t} \right] \tag{4.20}$$

as a sum over the same spherical harmonics as in (4.12). The time dependence is absent from the equations of motion and the conserved quantities, making it useful to define the

fields

$$h^{\pm}_{LM} \equiv h_{LM} \pm (-1)^M h^*_{L,-M} \ , \tag{4.21}$$

where

$$h^{\pm *}_{LM} = \pm (-1)^M h^{\pm}_{L,-M} \ . \tag{4.22}$$

We also express the angular momentum and charge of the soliton in terms of these fields. The above relations allow us to do so while only summing over $M \geq 0$. First, we find

$$J_z = \frac{\phi_0^2}{2} \sum_{L,M>0} M \int dr\, r^2 \left[\mu M \left(|h^+_{LM}|^2 + |h^-_{LM}|^2 \right) + \omega \left(h^{+*}_{LM} h^-_{LM} + h^{-*}_{LM} h^+_{LM} \right) \right] \ . \tag{4.23}$$

Note that we expect the angular momentum to vanish for $\mu = 0$ when $\omega > 0$. This is guaranteed to occur if either h^+_{LM} or h^-_{LM} goes to zero as $\mu \to 0$. We also find the charge

$$\begin{aligned} Q =& 4\pi\omega\phi_0^2 \int dr\, r^2 f^2 + \frac{\phi_0^2}{2} \sum_{L,M>0} \int dr\, r^2 \left[\omega \left(|h^+_{LM}|^2 + |h^-_{LM}|^2 \right) + \mu M \left(h^{+*}_{LM} h^-_{LM} + h^{-*}_{LM} h^+_{LM} \right) \right] \\ &+ \frac{\omega\phi_0^2}{4} \sum_L \int dr\, r^2 \left(|h^+_{L0}|^2 + |h^-_{L0}|^2 \right) \ . \end{aligned} \tag{4.24}$$

When $\mu \to 0$ the corrections to Q from this perturbation need not vanish. Such a scenario might correspond to the introduction of additional scalar field that does not carry angular momentum.

In general, the $h^{\pm}_{LM}$ of different (L, M) are all coupled since the equations of motion are

nonlinear. However, for small perturbations $h_{LM} \to \epsilon\, h_{LM}$ with $\epsilon \ll 1$, the ϵ^1 order functions decouple:

$$\begin{aligned} 0 = &\partial_\rho^2 h^+_{LM} + \frac{2}{\rho}\partial_\rho h^+_{LM} - \frac{L(L+1)}{\rho^2} h^+_{LM} + \left(\Omega^2 + M^2\overline{\mu}^2\right) h^+_{LM} + 2\Omega M\overline{\mu}\, h^-_{LM} \\ &- h^+_{LM}\phi_0^2 \left.\frac{\partial \overline{U}}{\partial(\Phi\Phi^*)}\right|_{\Phi=\Phi_0} - h^+_{LM} f^2 \phi_0^4 \left.\frac{\partial^2 \overline{U}}{\partial(\Phi\Phi^*)^2}\right|_{\Phi=\Phi_0}, \end{aligned} \tag{4.25}$$

$$\begin{aligned} 0 = &\partial_\rho^2 h^-_{LM} + \frac{2}{\rho}\partial_\rho h^-_{LM} - \frac{L(L+1)}{\rho^2} h^-_{LM} + \left(\Omega^2 + M^2\overline{\mu}^2\right) h^-_{LM} + 2\Omega M\overline{\mu}\, h^+_{LM} \\ &- h^-_{LM}\phi_0^2 \left.\frac{\partial \overline{U}}{\partial(\Phi\Phi^*)}\right|_{\Phi=\Phi_0}, \end{aligned} \tag{4.26}$$

where

$$\overline{\mu} = \frac{\mu}{\sqrt{m_\phi^2 - \omega_0^2}}\ . \tag{4.27}$$

For each (L, M), these are two real coupled differential equations. The leading order contributions to the energy are

$$\begin{aligned} E = &\frac{\phi_0^2}{2}\int dr r^2 \left[(\partial_r f)^2 + \omega^2 f^2 + U\left(f^2\right)\right] \\ &+ \epsilon^2 \frac{\phi_0^2}{4} \sum_{L,M>0} \int dr r^2 \left\{ \left|\partial_r h^+_{LM}\right|^2 + \left|\partial_r h^-_{LM}\right|^2 + 2M\omega\mu \left(h^{+*}_{LM} h^-_{LM} + h^{-*}_{LM} h^+_{LM}\right) \right. \\ &+ \left[\mu^2 M^2 + \omega^2 + \frac{L(L+1)}{r^2} + \left.\frac{\partial U}{\partial(\Phi\Phi^*)}\right|_{\Phi=\Phi_0}\right] \left(|h^+_{LM}|^2 + |h^-_{LM}|^2\right) \\ &\left. + 2\Phi_0^2 \left|h^+_{LM}\right|^2 \left.\frac{\partial^2 U}{\partial(\Phi\Phi^*)^2}\right|_{\Phi=\Phi_0} \right\} + \epsilon^2 \frac{\phi_0^2}{8} \sum_L \int dr r^2 \left\{ \left|\partial_r h^+_{L0}\right|^2 + \left|\partial_r h^-_{L0}\right|^2 \right. \\ &\left. + \left[\omega^2 + \frac{L(L+1)}{r^2} + \left.\frac{\partial U}{\partial(\Phi\Phi^*)}\right|_{\Phi=\Phi_0}\right] \left(|h^+_{L0}|^2 + |h^-_{L0}|^2\right) + 2\Phi_0^2 \left|h^+_{L0}\right|^2 \left.\frac{\partial^2 U}{\partial(\Phi\Phi^*)^2}\right|_{\Phi=\Phi_0} \right\}\ . \end{aligned} \tag{4.28}$$

We emphasize that at this point the perturbation parameter ϵ used here captures both corrections with angular momentum and those without.

To obtain solutions that correspond to small angular momentum, we further expand each $h^{\pm}_{LM}$ in a power series in $\overline{\mu}$. We note that $\overline{\mu} \to -\overline{\mu}$ leaves the equations of motion invariant if combined with $h^{\pm}_{LM} \to \pm h^{\pm}_{LM}$. The expansion therefore has the form

$$h^{+}_{LM} = h^{+(0)}_{LM} + \overline{\mu}^2 h^{+(2)}_{LM} + \dots \tag{4.29}$$

$$h^{-}_{LM} = \overline{\mu}\, h^{-(1)}_{LM} + \overline{\mu}^3 h^{-(3)}_{LM} + \dots \ . \tag{4.30}$$

In particular, we see that h^{+}_{LM} can be nonzero even when $\overline{\mu} \to 0$. By a nearly identical argument we see that $h^{\pm}_{L,-M} = \pm h^{\pm}_{LM}$. We set all $h_{L0} = 0$ since these modes do not contribute to J_z even for nonzero $\overline{\mu}$.

To zeroth order in $\overline{\mu}$, the h^{+}_{LM} equation is

$$\begin{aligned} 0 = {} & \partial_\rho^2 h^{+(0)}_{LM} + \frac{2}{\rho}\partial_\rho h^{+(0)}_{LM} - \frac{L(L+1)}{\rho^2} h^{+(0)}_{LM} + \Omega^2 h^{+(0)}_{LM} \\ & - h^{+(0)}_{LM} \left[\phi_0^2 \frac{\partial \overline{U}}{\partial(\Phi\Phi^*)} + f^2 \phi_0^4 \frac{\partial^2 \overline{U}}{\partial(\Phi\Phi^*)^2} \right]_{\Phi=\Phi_0} . \end{aligned} \tag{4.31}$$

To find a solution, we take the ρ derivative of Eq. (4.3) and find

$$0 = -\Omega^2 \partial_\rho f - \partial_\rho^3 f - \frac{2}{\rho}\partial_\rho^2 f + \frac{2}{\rho^2}\partial_\rho f + \partial_\rho f \phi_0^2 \frac{\partial \overline{U}}{\partial(\Phi_0 \Phi_0^*)} + \phi_0^4 f^2 \partial_\rho f \frac{\partial^2 \overline{U}}{\partial(\Phi_0 \Phi_0^*)^2} \, . \tag{4.32}$$

This shows that there is an *exact* solution of Eq. (4.31) for $L = 1$:

$$h^{+(0)}_{1,\pm 1} = c_1 \partial_\rho f \, , \tag{4.33}$$

where the constant c_1 must be purely imaginary to satisfy Eq. (4.22). As the magnitude is arbitrary at this order in ϵ, we simply take $c_1 =$i.

To first order in $\bar{\mu}$, the equation for h_{11}^{-} is

$$\partial_\rho^2 h_{1,\pm1}^{-(1)} + \frac{2}{\rho}\partial_\rho h_{1,\pm1}^{-(1)} - \frac{2}{\rho^2} h_{1,\pm1}^{-(1)} + \Omega^2 h_{1,\pm1}^{-(1)} - h_{1,\pm1}^{-(1)}\phi_0^2 \left.\frac{\partial \overline{U}}{\partial(\Phi\Phi^*)}\right|_{\Phi=\Phi_0} = \mp\, 2\mathrm{i}\omega\partial_\rho f\,. \tag{4.34}$$

One can verify, using Eq. (4.3), that this is solved by

$$h_{1,\pm1}^{-(1)} = \mp\,\mathrm{i}\Omega\,\rho f\ . \tag{4.35}$$

Thus for $L = 1$ we have found a solution up to order $\overline{\mu}$

$$h_{1,\pm1}^{+} = \mathrm{i}\partial_\rho f\,, \qquad\qquad h_{1,\pm1}^{-} = \mp\mathrm{i}\overline{\mu}\,\Omega\,\rho f\,. \tag{4.36}$$

We illustrate these profiles in the left panel of Fig. 4.1 for a sextic potential, but emphasize that the solution holds for any potential that supports Q-balls. For this configuration the $\epsilon^2\overline{\mu}^0$ contribution to the energy density, as calculated in what follows, has the form given in the right panel of Fig. 4.1. Note that because the energy is independent of the direction of rotation the first $\overline{\mu}$ dependence comes at order $\overline{\mu}^2$. To obtain the complete correction to this order we would also need the $\overline{\mu}^2$ contribution to $h_{1,\pm1}^{+}$.

Now, the unperturbed solution (with $J_z = 0$) has particle number and energy [1] given by

$$Q_0 = \frac{4\pi\Omega\phi_0^2}{m_\phi^2 - \omega_0^2}\int \mathrm{d}\rho\,\rho^2 f^2\,, \tag{4.37}$$

$$E_0 = \omega Q_0 + \frac{4\pi\phi_0^2}{3\sqrt{m_\phi^2 - \omega_0^2}}\int \mathrm{d}\rho\,\rho^2\,(\partial_\rho f)^2\,. \tag{4.38}$$

The first term in the energy scales like the volume of the Q-ball, while the second scales like the surface area and so is typically subleading for large Q-balls.

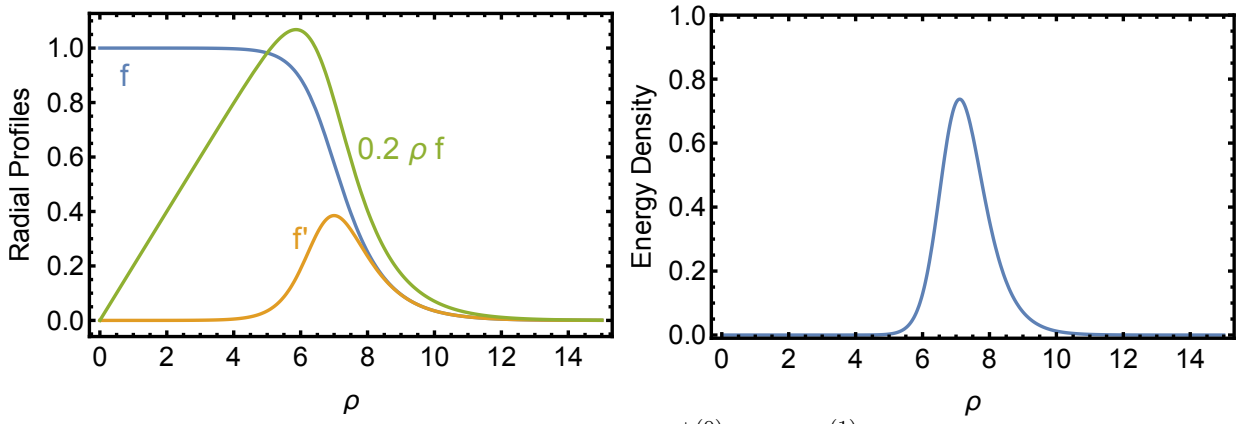

Figure 4.1: (Left) Illustration of the radial profiles f, $h^{+(0)}_{1,-1}$, and $h^{-(1)}_{1,-1}$ and (right) the $\epsilon^2\overline{\mu}^0$ correction to the energy density for the sextic potential of Ref. [1]. The normalization of the perturbations, including the correction to the energy density, is has been adjust to make them fit easily on the same figure.

Using the pertubative solution given above we find that the pertubation contributes an angular momentum that is positive for $\overline{\mu} > 0$ and to leading order is

$$\begin{aligned}\Delta J_z =& \frac{\phi_0^2\overline{\mu}\epsilon^2}{m_\phi^2-\omega_0^2}\int \mathrm{d}\rho\,\rho^2\left[(\partial_\rho f)^2+3\Omega^2 f^2\right]+\mathcal{O}(\epsilon^2\overline{\mu}^2)\\ =&\overline{\mu}\epsilon^2\frac{3}{4\pi}\frac{E_0}{\sqrt{m_\phi^2-\omega_0^2}}+\mathcal{O}(\epsilon^2\overline{\mu}^3)\,.\end{aligned} \tag{4.39}$$

with $J_{x,y}=0$. We also find that the charge is shifted from Q_0 by a positive amount

$$\Delta Q = \epsilon^2\frac{3}{4\pi}\frac{E_0-\omega Q_0}{\sqrt{m_\phi^2-\omega_0^2}}+\mathcal{O}(\epsilon^2\overline{\mu}^2) \tag{4.40}$$

and the energy is shifted from the nonrotating value by

$$\Delta E = \omega\Delta Q+\mathcal{O}(\epsilon^2\overline{\mu}^2)\,. \tag{4.41}$$

Notice that, unlike the angular momentum, the leading $\overline{\mu}$ corrections to the charge and energy go like $\overline{\mu}^2$ so our linear in rotation solution does not capture all the possible energy corrections to leading order.

We also compare the energy of the localized solution to one in which the added charge ΔQ is spread at infinity with zero kinetic energy and hence has $\Delta E = m_\phi \Delta Q$. This delocalized solution has higher energy as long as $\omega < m_\phi$ (which is always true for a Q-ball). This indicates that when the higher order terms can be consistently set to zero that the rotating perturbative solution is stable against dissociation.

4.4 Higher Orders in ϵ

At linear order in ϵ the system of Eq. (4.25) and Eq. (4.26) is solvable, as illustrated above, as a perturbation series in $\overline{\mu}$. Issues arise at higher order in ϵ, where the non-linearities in the Q-ball potential couple the different (L, M) modes and enforce an infinite set of non-vanishing h_{LM}.

Exterior to the Q-ball, at large r, the relevant differential equation of some higher-ϵ mode takes the form

$$\partial_r^2 h_{LM} + \frac{2}{r}\partial_r h_{LM} - \frac{L(L+1)}{r^2} h_{LM} + \left(\omega^2 - m_\phi^2 + M^2\mu^2\right) h_{LM} \approx 0\,, \tag{4.42}$$

where exponentially suppressed terms have been dropped on the right hand side. As shown in App. A.2, for almost all Q-balls consistency requires infinitely many (L, M) modes. At large M, the expression $\omega^2 - m_\phi^2 + M^2\mu^2$ becomes positive and no longer admits localized solutions, but rather corresponds to radiation modes that indicate an instability.

In this case the solutions to Eq. (4.42) are spherical Bessel functions. However, we are primarily interested in their large-r form

$$h_{LM} \sim \frac{1}{r\sqrt{\omega^2 - m_\phi^2 + M^2\mu^2}} \cos\left(r\sqrt{\omega^2 - m_\phi^2 + M^2\mu^2} - L\frac{\pi}{2}\right)\,. \tag{4.43}$$

As shown below, because these field fall off like $1/r$ they lead to nonzero radiated power.

While this conclusion is fairly straightforward, we highlight a subtle feature: the right-hand side in Eq. (4.42) is of course not zero, but rather exponentially suppressed by the lower-ϵ source terms. The resulting *inhomogeneous* differential equation could conceivably have a localized solution, allowing us to drop the oscillating solution to the *homogeneous* equation. The answer to this question lies beyond the scope of this article, in the following we work under the conservative assumption that the classical slowly-rotating Q-ball solution is indeed unstable.

The lifetime of these solitons is impossible to calculate exactly without calculating the perturbative series up to the order nonlocalized functions are sourced. To estimate the lifetime of the rotating perturbation to the spherical Q-ball solution we separate the perturbation into two parts: the localized field and the radiating field. This radiating field carries angular momentum and energy away from the localized field configuration. Similar to the Poynting vector analysis in electromagnetism, the radiated power carried by the nonlocalized modes at an instant in time is determined by

$$\mathcal{P} = \int \mathrm{d}\theta \, \mathrm{d}\varphi \, r^2 \sin\theta \, T^{0r} \Big|_{r\to\infty} \, , \tag{4.44}$$

where the energy-momentum tensor is

$$T_{\mu\nu} = \partial_\mu(\Phi^*)\partial_\nu\Phi + \partial_\nu(\Phi^*)\partial_\mu\Phi - \eta_{\mu\nu}\left[\partial_\alpha(\Phi^*)\partial^\alpha\Phi - U(\Phi^*\Phi)\right] \, . \tag{4.45}$$

This leads to

$$\mathcal{P} = \int \mathrm{d}\theta\, \mathrm{d}\varphi\, r^2 \sin\theta \left[\mathrm{i}\omega \left(\Phi\partial_r\Phi^* - \Phi^*\partial_r\Phi\right) + \mu \left(\partial_\varphi(\Phi^*)\partial_r\Phi + \partial_r(\Phi^*)\partial_\varphi\Phi\right)\right]\Big|_{r\to\infty} . \quad (4.46)$$

The integration is of a quadratic function of the fields over the surface at infinity.

The scalar field determined in the previous section has the form

$$\Phi = \text{localized} + \mathcal{O}(\epsilon^2) + \mathcal{O}(\epsilon\overline{\mu}^2) \ . \quad (4.47)$$

In other words, we have only established that the full perturbative solution is localized to a low order in our expansion parameters ϵ and $\overline{\mu}$. These localized fields do not contribute to any radiated power. Thus, we conclude that the radiated power, which would need two powers of functions that fall off like $1/r$, goes like

$$\mathcal{P} = 0 + \mathcal{O}(\epsilon^4) + \mathcal{O}(\epsilon^2\overline{\mu}^4) + \mathcal{O}(\epsilon^3\overline{\mu}^2) \ . \quad (4.48)$$

Here ϵ, $\overline{\mu} \ll 1$, so the radiated power is small. This allows us to estimate the total time to radiate away all the energy ΔE and angular momentum of the rotating state as

$$\Delta t \sim \frac{\Delta E}{\mathcal{P}} \sim \frac{1}{\mathcal{O}(\epsilon^2) + \mathcal{O}(\overline{\mu}^4) + \mathcal{O}(\epsilon\overline{\mu}^2)}, \quad (4.49)$$

where we have taken the increase of energy from the spinning state to go like ϵ^2, as explicitly

calculated in the previous section.[3] For small ϵ and $\overline{\mu}$ this time can be arbitrarily long, rendering these field configurations classically metastable.

The eventual decay may be understood as follows: in a classical universe, a rotating Q-ball can reduce its angular momentum by emitting an arbitrarily small amount of charge, which can carry an arbitrarily large angular momentum if it moves far away from the Q-ball with a small angular velocity. If the emitted charge can be made arbitrarily small, the binding energy is also small, and this emission is energetically favorable. While this picture is plausible, it does not distinguish between the known solutions with quantized angular momenta and the small angular momenta configurations we are exploring. We leave the full understanding of rotating Q-ball stability to future work.

4.5 Conclusion

In this chapter we examine slowly rotating Q-balls.[4] We construct a more general ansatz that allows us to consider perturbative extensions of known Q-ball solutions whose angular momentum need not satisfy $J = NQ$. A localized, leading-order perturbative correction is found which applies to all theories that give rise to Q-balls. We further show that this perturbative solution has lower energy than the unperturbed Q-ball surrounded by a free scalar field at infinity and hence is stable against dissociation.

In general, Q-ball potentials produce non-linearities in the equation of motion which require higher order modes to be nonzero. We have shown that this suggests the existence of a non-local, hence radiating, portion of the scalar field. For small rotation, however, these radiation modes are only required to appear at subleading order in the expansion parameter.

[3] This follows from the largest shift to the energy coming from the leading order ϵ correction rather than the higher order terms that might contribute to radiation.

[4] Previous perturbative analyses of *boson stars* were not sufficiently general to allow for scalar fields with angular momentum.

Therefore, though the localized perturbation is only an approximate solution to the equations of motion, the approximation can be quite close to a true solution. We estimate the life-time of the localized perturbation from the radiated power contained in the non-localized part of the field. We find that small angular momentum solitons are classically metastable in the small angular velocity limit with lifetimes that can be relevant to cosmological studies.

Therefore, we have meaningfully expanded the possibilities for rotating Q-balls. This is not simply a formal question; there are important phenomenological consequences. Specifically, the existence of this new class of long-lived, slowly rotating Q-ball perturbations enhances the validity of standard calculations of the Q-ball relic density; without these rotating states, only Q-balls with specific values of the angular momentum would be produced, and the relic density would presumably be much smaller. A full analysis requires further investigation into the dynamics of rotating Q-balls and their localized perturbations.

There are many other questions regarding rotating Q-balls. We focused on small angular velocities in order to explore the dynamics of rotating Q-balls in this limit. It would be interesting to have an improved characterization of these solutions for arbitrary angular momentum, perhaps using the methods of [77, 78]. Extending these solutions to boson stars, oscillons, axion stars, and other solitons in the literature would also be very interesting. Also, studying rotating Q-balls in a full quantum mechanical theory would be worth investigating as this might significantly affect their stability. We hope to return to these questions in future work.

Chapter 5

Overall Conclusion

Q-balls are intriguing example of stable non-topological solitons, which are well-motivated from field theory. As discussed in the Chapter 1, the relevance of Q-balls extends beyond theoretical curiosities and could be related to pivotal phenomenological questions in particle physics. However, in order to build a testable phenomenological Q-ball model, it is crucial to analyze the full space of these solutions. Therefore, in this dissertation, we try to explore theoretical aspects about Q-balls that have not been fully addressed in the literature.

In Chapter 2 and 3, we discuss radial excitation modes of global and gauged Q-ball to provide a complete picture of the solution space of Q-ball in the sextic potential. In Chapter 2, excited global Q-balls properties are analytically analyzed. Radii of these excitation modes are derived analytically, which allows us to approximate the profiles of these modes as products of transition functions in the thin-wall limit. We show that despite the richer structure of the excited states compared to the ground states of global Q-balls, the properties such as the charge and energy of the excitation modes can be approximated with a single length scale similar to the ground state. We build on this observation in Chapter 3 as we discuss gauged Q-balls. Gauged Q-balls are harder to solve due to having to two coupled non-

linear differential equations. However, an interesting mapping relation between global and gauged Q-balls emerges when looking closely at the differential equations as shown in [4]. We extend this mapping relation to study excited gauged Q-balls, and this successfully enables us to describe the excitation modes of gauged Q-balls. This is illustrated numerically by using the finite element method to generate excited gauged Q-balls profiles, and analytically by deriving expression for properties in the thin-wall limits. We comment on the instability of the radial excited global and gauged Q-ball.

In Chapter 4, we explore the possible existence of slowly rotating Q-balls. While Q-balls are macroscopic classical objects, their angular momentum is traditionally treated in the literature as an integer multiple of the charge. We challenge this assumption by working with a general Q-ball ansatz that admits perturbation of arbitrarily small angular momentum. A metastable slowly rotating Q-ball solution has been shown to exist in terms of a leading-order localized perturbation. This enlarges the solution space of rotating Q-balls.

Bibliography

[1] Julian Heeck, Arvind Rajaraman, Rebecca Riley, and Christopher B. Verhaaren. Understanding Q-Balls Beyond the Thin-Wall Limit. *Phys. Rev.*, D103:045008, 2021.

[2] Yahya Almumin, Julian Heeck, Arvind Rajaraman, and Christopher B. Verhaaren. Excited Q-balls. *Eur. Phys. J. C*, 82(9):801, 2022.

[3] Yahya Almumin, Julian Heeck, Arvind Rajaraman, and Christopher B. Verhaaren. Slowly rotating Q-balls. *Eur. Phys. J. C*, 84(4):364, 2024.

[4] Julian Heeck, Arvind Rajaraman, Rebecca Riley, and Christopher B. Verhaaren. Mapping Gauged Q-Balls. *Phys. Rev. D*, 103(11):116004, 2021.

[5] Sidney R. Coleman. Q Balls. *Nucl. Phys.*, B262:263, 1985. [Erratum: Nucl. Phys. B269, 744 (1986)].

[6] Alexander Kusenko. Solitons in the supersymmetric extensions of the standard model. *Phys. Lett. B*, 405:108, 1997.

[7] Kari Enqvist and John McDonald. Q balls and baryogenesis in the MSSM. *Phys. Lett. B*, 425:309–321, 1998.

[8] Durmus A. Demir. Stable Q balls from extra dimensions. *Phys. Lett. B*, 495:357–362, 2000.

[9] Steven Abel and Alex Kehagias. Q-branes. *JHEP*, 11:096, 2015.

[10] Fady Bishara, George Johnson, Olivier Lennon, and John March-Russell. Higgs Assisted Q-balls from Pseudo-Nambu-Goldstone Bosons. *JHEP*, 11:179, 2017.

[11] Fady Bishara and Olivier Lennon. Thin-Walled Higgs Assisted Q-balls from Pseudo-Nambu-Goldstone Bosons. 10 2021.

[12] E. Krylov, A. Levin, and V. Rubakov. Cosmological phase transition, baryon asymmetry and dark matter Q-balls. *Phys. Rev.*, D87:083528, 2013.

[13] Alexander Kusenko and Anupam Mazumdar. Gravitational waves from fragmentation of a primordial scalar condensate into Q-balls. *Phys. Rev. Lett.*, 101:211301, 2008.

[14] Djuna Croon, Alexander Kusenko, Anupam Mazumdar, and Graham White. Solitosynthesis and Gravitational Waves. *Phys. Rev.*, D101:085010, 2020.

[15] Richard Battye and Paul Sutcliffe. Q-ball dynamics. *Nucl. Phys. B*, 590:329–363, 2000.

[16] Tuomas Multamaki and Iiro Vilja. Simulations of Q ball formation. *Phys. Lett. B*, 535:170–176, 2002.

[17] Mitsuo I. Tsumagari. Affleck-Dine dynamics, Q-ball formation and thermalisation. *Phys. Rev. D*, 80:085010, 2009.

[18] Takashi Hiramatsu, Masahiro Kawasaki, and Fuminobu Takahashi. Numerical study of Q-ball formation in gravity mediation. *JCAP*, 06:008, 2010.

[19] Alexander Kusenko and Mikhail E. Shaposhnikov. Supersymmetric Q balls as dark matter. *Phys. Lett.*, B418:46–54, 1998.

[20] Alexander Kusenko, Vadim Kuzmin, Mikhail E. Shaposhnikov, and P.G. Tinyakov. Experimental signatures of supersymmetric dark matter Q balls. *Phys. Rev. Lett.*, 80:3185–3188, 1998.

[21] Alexander Kusenko and Paul J. Steinhardt. Q ball candidates for selfinteracting dark matter. *Phys. Rev. Lett.*, 87:141301, 2001.

[22] Eduardo Pontón, Yang Bai, and Bithika Jain. Electroweak Symmetric Dark Matter Balls. *JHEP*, 09:011, 2019.

[23] Yang Bai and Joshua Berger. Nucleus Capture by Macroscopic Dark Matter. *JHEP*, 05:160, 2020.

[24] Yang Bai, Sida Lu, and Nicholas Orlofsky. Q-monopole-ball: a topological and non-topological soliton. *JHEP*, 01:109, 2022.

[25] Ali Masoumi, Ken D. Olum, and Benjamin Shlaer. Efficient numerical solution to vacuum decay with many fields. *JCAP*, 1701:051, 2017.

[26] G. Rosen. Dilatation covariance and exact solutions in local relativistic field theories. *Phys. Rev.*, 183:1186–1188, 1969.

[27] Stavros Theodorakis. Analytic Q ball solutions in a parabolic-type potential. *Phys. Rev.*, D61:047701, 2000.

[28] R.B. MacKenzie and Manu B. Paranjape. From Q-walls to Q-balls. *JHEP*, 08:003, 2001.

[29] I. E. Gulamov, E. Ya. Nugaev, and M. N. Smolyakov. Analytic Q-ball solutions and their stability in a piecewise parabolic potential. *Phys. Rev.*, D87:085043, 2013.

[30] Julian Heeck, Arvind Rajaraman, Rebecca Riley, and Christopher B. Verhaaren. Proca Q-balls and Q-shells. *JHEP*, 10:103, 2021.

[31] Mikhail S. Volkov and Erik Wohnert. Spinning Q balls. *Phys. Rev. D*, 66:085003, 2002.

[32] Manuel Mai and Peter Schweitzer. Radial excitations of Q-balls, and their D-term. *Phys. Rev. D*, 86:096002, 2012.

[33] Tuomas Multamaki. Excited Q balls in the MSSM with gravity mediated supersymmetry breaking. *Phys. Lett. B*, 511:92–100, 2001.

[34] Edmund J. Copeland, Paul M. Saffin, and Shuang-Yong Zhou. Charge-Swapping Q-balls. *Phys. Rev. Lett.*, 113:231603, 2014.

[35] Qi-Xin Xie, Paul M. Saffin, and Shuang-Yong Zhou. Charge-Swapping Q-balls and Their Lifetimes. *JHEP*, 07:062, 2021.

[36] Si-Yuan Hou, Paul M. Saffin, Qi-Xin Xie, and Shuang-Yong Zhou. Charge-swapping Q-balls in a logarithmic potential and Affleck-Dine condensate fragmentation. *JHEP*, 07:060, 2022.

[37] Qi-Xin Xie, Paul M. Saffin, Anders Tranberg, and Shuang-Yong Zhou. Quantum corrected Q-ball dynamics. *JHEP*, 01:165, 2024.

[38] L. Campanelli and M. Ruggieri. Spinning Supersymmetric Q-balls. *Phys. Rev. D*, 80:036006, 2009.

[39] H. Arodz, J. Karkowski, and Z. Swierczynski. Spinning Q-balls in the complex signum-Gordon model. *Phys. Rev. D*, 80:067702, 2009.

[40] Ya Shnir. Q-vortices, Q-walls and coupled Q-balls. *J. Phys. A*, 44:425202, 2011.

[41] E. Nugaev and A. Shkerin. Investigation of Q-tubes stability using the piecewise parabolic potential. *Phys. Rev. D*, 90(1):016002, 2014.

[42] V. Loiko, I. Perapechka, and Ya. Shnir. Q-balls without a potential. *Phys. Rev. D*, 98:045018, 2018.

[43] Vanda Silveira and Claudio M. G. de Sousa. Boson star rotation: A Newtonian approximation. *Phys. Rev. D*, 52:5724–5728, 1995.

[44] Burkhard Kleihaus, Jutta Kunz, and Meike List. Rotating boson stars and Q-balls. *Phys. Rev. D*, 72:064002, 2005.

[45] Burkhard Kleihaus, Jutta Kunz, Meike List, and Isabell Schaffer. Rotating Boson Stars and Q-Balls. II. Negative Parity and Ergoregions. *Phys. Rev. D*, 77:064025, 2008.

[46] Burkhard Kleihaus, Jutta Kunz, and Stefanie Schneider. Stable Phases of Boson Stars. *Phys. Rev. D*, 85:024045, 2012.

[47] Steven L. Liebling and Carlos Palenzuela. Dynamical Boson Stars. *Living Rev. Rel.*, 15:6, 2012.

[48] Sacha Davidson and Thomas Schwetz. Rotating Drops of Axion Dark Matter. *Phys. Rev. D*, 93:123509, 2016.

[49] C. Herdeiro, I. Perapechka, E. Radu, and Ya. Shnir. Asymptotically flat spinning scalar, Dirac and Proca stars. *Phys. Lett. B*, 797:134845, 2019.

[50] Lucas G. Collodel, Burkhard Kleihaus, and Jutta Kunz. Structure of rotating charged boson stars. *Phys. Rev. D*, 99:104076, 2019.

[51] Jorge F. M. Delgado, Carlos A. R. Herdeiro, and Eugen Radu. Rotating Axion Boson Stars. *JCAP*, 06:037, 2020.

[52] Felix Kling, Arvind Rajaraman, and Freida Liz Rivera. New solutions for rotating boson stars. *Phys. Rev. D*, 103:075020, 2021.

[53] A. S. Dmitriev, D. G. Levkov, A. G. Panin, E. K. Pushnaya, and I. I. Tkachev. Instability of rotating Bose stars. *Phys. Rev. D*, 104(2):023504, 2021.

[54] Romain Gervalle. Chains of rotating boson stars. *Phys. Rev. D*, 105:124052, 2022.

[55] Nils Siemonsen and William E. East. Binary boson stars: Merger dynamics and formation of rotating remnant stars. *Phys. Rev. D*, 107:124018, 2023.

[56] Kim Griest, Edward W. Kolb, and Alessandro Massarotti. Statistical Fluctuations as the Origin of Nontopological Solitons. *Phys. Rev. D*, 40:3529, 1989.

[57] Kim Griest and Edward W. Kolb. Solitosynthesis: Cosmological Evolution of Nontopological Solitons. *Phys. Rev. D*, 40:3231, 1989.

[58] Marieke Postma. Solitosynthesis of Q balls. *Phys. Rev.*, D65:085035, 2002.

[59] R. Friedberg, T. D. Lee, and A. Sirlin. A Class of Scalar-Field Soliton Solutions in Three Space Dimensions. *Phys. Rev.*, D13:2739–2761, 1976.

[60] A. Yu. Loginov and V. V. Gauzshtein. Radially excited $U(1)$ gauged Q-balls. *Phys. Rev.*, D102:025010, 2020.

[61] Alexander Kusenko. Small Q balls. *Phys. Lett. B*, 404:285, 1997.

[62] F. Paccetti Correia and M. G. Schmidt. Q balls: Some analytical results. *Eur. Phys. J. C*, 21:181–191, 2001.

[63] T. D. Lee and Y. Pang. Nontopological solitons. *Phys. Rept.*, 221:251–350, 1992.

[64] Mitsuo I. Tsumagari, Edmund J. Copeland, and Paul M. Saffin. Some stationary properties of a Q-ball in arbitrary space dimensions. *Phys. Rev. D*, 78:065021, 2008.

[65] I.E. Gulamov, E.Ya. Nugaev, and M.N. Smolyakov. Theory of $U(1)$ gauged Q-balls revisited. *Phys. Rev. D*, 89:085006, 2014.

[66] Ki-Myeong Lee, Jaime A. Stein-Schabes, Richard Watkins, and Lawrence M. Widrow. Gauged Q Balls. *Phys. Rev.*, D39:1665, 1989.

[67] I. E. Gulamov, E. Ya. Nugaev, A. G. Panin, and M. N. Smolyakov. Some properties of $U(1)$ gauged Q-balls. *Phys. Rev.*, D92:045011, 2015.

[68] Yves Brihaye, Adolfo Cisterna, Betti Hartmann, and Gabriel Luchini. From topological to nontopological solitons: Kinks, domain walls, and Q-balls in a scalar field model with a nontrivial vacuum manifold. *Phys. Rev. D*, 92(12):124061, 2015.

[69] A. Yu. Loginov and V. V. Gauzshtein. Radially excited $U(1)$ gauged Q-balls. *Phys. Rev. D*, 102(2):025010, 2020.

[70] A. G. Panin and M. N. Smolyakov. Problem with classical stability of U(1) gauged Q-balls. *Phys. Rev. D*, 95:065006, 2017.

[71] Wolfram Research, Inc. Mathematica, Version 12.2. Champaign, IL, 2020.

[72] Y. Kobayashi, M. Kasai, and T. Futamase. Does a boson star rotate? *Phys. Rev. D*, 50:7721–7724, 1994.

[73] Franz E. Schunck and Eckehard W. Mielke. *Rotating Boson Stars*, pages 138–151. Springer Berlin Heidelberg, Berlin, Heidelberg, 1996.

[74] France E. Schunck and Eckehard W. Mielke. Rotating boson star as an effective mass torus in general relativity. *Phys. Lett. A*, 249:389–394, 1998.

[75] Eugen Radu and Mikhail S. Volkov. Existence of stationary, non-radiating ring solitons in field theory: knots and vortons. *Phys. Rept.*, 468:101–151, 2008.

[76] Eugen Radu and Mikhail S. Volkov. Spinning Electroweak Sphalerons. *Phys. Rev. D*, 79:065021, 2009.

[77] Felix Kling and Arvind Rajaraman. Towards an Analytic Construction of the Wavefunction of Boson Stars. *Phys. Rev. D*, 96:044039, 2017.

[78] Felix Kling and Arvind Rajaraman. Profiles of boson stars with self-interactions. *Phys. Rev. D*, 97:063012, 2018.

Appendix A

Slowly Rotating Q-balls

A.1 Angular Velocity

In this appendix we demonstrate in what sense μ can be interpreted as the angular velocity of the soliton. The angular momentum M is defined in terms of the energy momentum tensor T by

$$M^{ij} = \int d^3x \left(x^i T^{j0} - x^j T^{i0} \right) \ , \tag{A.1}$$

where in Cartesian coordinates $J_x = M^{23}$, $J_y = -M^{13}$, and $J_z = M^{12}$. This leads to

$$J_x = \int \mathrm{d}^3x \left[\dot{\Phi} \left(\sin\varphi \partial_\theta + \frac{\cos\varphi}{\tan\theta} \partial_\varphi \right) \Phi^* + \dot{\Phi}^* \left(\sin\varphi \partial_\theta + \frac{\cos\varphi}{\tan\theta} \partial_\varphi \right) \Phi \right] \ , \tag{A.2}$$

$$J_y = \int \mathrm{d}^3x \left[\dot{\Phi} \left(-\cos\varphi \partial_\theta + \frac{\sin\varphi}{\tan\theta} \partial_\varphi \right) \Phi^* + \dot{\Phi}^* \left(-\cos\varphi \partial_\theta + \frac{\sin\varphi}{\tan\theta} \partial_\varphi \right) \Phi \right] \ , \tag{A.3}$$

$$J_z = -\int \mathrm{d}^3x \left[\dot{\Phi} \partial_\varphi \Phi^* + \dot{\Phi}^* \partial_\varphi \Phi \right] \ . \tag{A.4}$$

Note that from these results we quickly see that for an axisymmetric field $\Phi(r,\theta)$ we have

$$J_x = \int \mathrm{d}r\mathrm{d}\theta r^2 \sin\theta \left(\dot{\Phi}\partial_\theta\Phi^* + \dot{\Phi}^*\partial_\theta\Phi\right)\int_0^{2\pi} d\varphi \sin\varphi = 0 \tag{A.5}$$

$$J_y = -\int \mathrm{d}r\mathrm{d}\theta r^2 \sin\theta \left(\dot{\Phi}\partial_\theta\Phi^* + \dot{\Phi}^*\partial_\theta\Phi\right)\int_0^{2\pi} d\varphi \cos\varphi = 0 \tag{A.6}$$

$$J_z = 0 \ . \tag{A.7}$$

This shows that an axisymmetric scalar field configuration has zero angular momentum.

Using the relation given in Eq. (4.11) and the above definitions of the components of angular momentum we find

$$\begin{aligned}
\frac{\mathrm{d}J_x}{\mathrm{d}t} =& \int \mathrm{d}^3x \Big\{ \left(-i\omega\dot{\Phi} - \mu\partial_\varphi\dot{\Phi}\right)\left(\sin\varphi\partial_\theta + \frac{\cos\varphi}{\tan\theta}\partial_\varphi\right)\Phi^* \\
&+ \dot{\Phi}\left(\sin\varphi\partial_\theta + \frac{\cos\varphi}{\tan\theta}\partial_\varphi\right)\left(i\omega\Phi^* - \mu\partial_\varphi\Phi^*\right) \\
&+ \left(i\omega\dot{\Phi}^* - \mu\partial_\varphi\dot{\Phi}^*\right)\left(\sin\varphi\partial_\theta + \frac{\cos\varphi}{\tan\theta}\partial_\varphi\right)\Phi \\
&+ \dot{\Phi}^*\left(\sin\varphi\partial_\theta + \frac{\cos\varphi}{\tan\theta}\partial_\varphi\right)\left(-i\omega\Phi - \mu\partial_\varphi\Phi\right)\Big\} \\
=& \mu\int \mathrm{d}^3x \left\{\dot{\Phi}\left(\cos\varphi\partial_\theta - \frac{\sin\varphi}{\tan\theta}\partial_\varphi\right)\Phi^* + \dot{\Phi}^*\left(\cos\varphi\partial_\theta - \frac{\sin\varphi}{\tan\theta}\partial_\varphi\right)\Phi\right\} \\
=& -\mu J_y \ ,
\end{aligned} \tag{A.8}$$

where in the second equality we have integrated by parts to change $\partial_\varphi\dot{\Phi}$ to $\dot{\Phi}$. By a similar calculation we find

$$\frac{\mathrm{d}J_y}{\mathrm{d}t} = \mu J_x \ , \tag{A.9}$$

$$\frac{\mathrm{d}J_z}{\mathrm{d}t} = -\int \mathrm{d}^3x\partial_\varphi\left[|\dot{\Phi}|^2 - \omega^2|\Phi|^2 + \mu^2\left|\partial_\varphi\Phi\right|^2\right] = 0 \ . \tag{A.10}$$

This confirms the results in Eq. (4.19) that μ appears as the angular velocity about the z-axis in the Euler equations for rigid rotation.

A.2 Radiation Modes

In this appendix we give a more detailed discussion of the non-linearities that couple different (L, M) modes, as mentioned in Sec. 4.4. At higher orders in ϵ, nonlinear terms induce higher modes with larger values of M of the form (4.12). This can be seen more clearly by considering the following alternate expansion of Φ

$$\Phi = e^{\mathrm{i}\omega t} \sum_{n=-\infty}^{\infty} c_n(r,\theta) e^{\mathrm{i}n(\varphi-\mu t)} \ , \tag{A.11}$$

where the time dependence has been chosen so that Eq. (4.11) is satisfied. Within the Lagrangian we can consider how the c_n are linked by the potential through non-linear terms like

$$\int \mathrm{d}\varphi \left(|\Phi|^2\right)^N = \int \mathrm{d}\varphi \prod_{i=1}^{N} \sum_{n_i=\infty}^{\infty} \sum_{m_i=-\infty}^{\infty} c_{n_i} c^*_{m_i} e^{\mathrm{i}\varphi(n_i-m_i)} e^{\mathrm{i}\mu t(m_i-n_i)} \ . \tag{A.12}$$

When integrated over φ, terms containing

$$\exp\left\{\mathrm{i}\varphi\left(n_1 - m_1 + \ldots + n_N - m_N\right)\right\} \tag{A.13}$$

vanish unless

$$n_1 - m_1 + \ldots + n_N - m_N = 0 \ . \tag{A.14}$$

This ensures that the potential energy is time independent, but also generally couples low n modes to arbitrarily high n. An exceptional case is having only one nonzero c_n where

$$\int \mathrm{d}\varphi \left(|\Phi|^2\right)^N = 2\pi \left(|c_n|^2\right)^N \ . \tag{A.15}$$

In general the nth equation includes a source term from the potential

$$N \prod_{i=1}^{N-1} \sum_{n_i, m_i} c_{n_i} c^*_{m_i} c_{n+n_1-m_1+\ldots+n_i-m_i} \ . \tag{A.16}$$

Consider the simple case of $N = 2$ and suppose that two c_n are nonzero: c_a and c_b. The equation for some mode c_n includes the source term

$$2 \sum_{s,t} c_s c^*_t c_{n+s-t} \ . \tag{A.17}$$

This contributes to the $n = a$ and $n = b$ equations, but also sources the $n = 2a - b$ and $n = 2b - a$ modes. Therefore, we must take these modes to be nonzero, which in turn sources more modes, leading to n of larger and larger magnitude. One can show that the modes $n = a + N(b - a)$ and $n = b + N(a - b)$ are sourced for all integers N.

We can now determine at what order in ϵ higher M models are sourced. In general, this depends on the nature of the initial perturbative solution. Let us use, like the solution obtained in Sec. 4.3, a function which at order ϵ^0 is the nonrotating $M = 0$ (c_0) solution and the ϵ^1 solution has $L = 1$ with $M = \pm 1$ ($c_{\pm 1}$). This solution is exact to this order in perturbation theory.

The next Ms that are sourced are $M = \pm 2$ and these require the contributions of two $M = \pm 1$ modes, so they enter at ϵ^2. This pattern persists at each order in ϵ. Additional M terms require an $M - 1$ term coupled to a $M = \pm 1$ term through the potential. Thus, in general the $\pm M$ modes enter at order ϵ^M.